


Cite this: *RSC Adv.*, 2022, 12, 22004

# Synthesis and biological activity, and molecular modelling studies of potent cytotoxic podophyllotoxin-naphthoquinone compounds†

Ha Thanh Nguyen,<sup>\*ab</sup> Quynh Giang Nguyen Thi,<sup>ab</sup> Thu Ha Nguyen Thi,<sup>ab</sup> Phuong Hoang Thi,<sup>b</sup> Giang Le-Nhat-Thuy,<sup>ab</sup> Tuyet Anh Dang Thi,<sup>ab</sup> Bao Le-Quang,<sup>c</sup> Hai Pham-The<sup>ab</sup> and Tuyen Van Nguyen<sup>ab</sup>

A new approach for the synthesis of podophyllotoxin-naphthoquinone compounds using microwave-assisted three-component reactions is reported in this study. Novel podophyllotoxin-naphthoquinone derivatives with modification on ring E were synthesized. All the synthetic compounds were assessed in terms of their cytotoxicity profile against four cancer cell lines (KB, HepG2, A549, and MCF7), and noncancerous Hek-293 cell lines. Notably, treatment of SK-LU-1 cells with compounds **5a** and **5b** resulted in G2/M phase arrest of the cell cycle, caspase-3/7 activation, and apoptosis. Additionally, molecular docking studies were performed and showed important interaction of two compounds against residues in the colchicine-binding-site of tubulin as well. Taken together, compounds **5a** and **5b** were identified as potent anticancer agents.

Received 26th May 2022  
Accepted 27th July 2022

DOI: 10.1039/d2ra03312g

rsc.li/rsc-advances

## Introduction

Microtubules, generated through polymerization of heterodimers of  $\alpha$ , $\beta$ -tubulins, have been an attractive target in the development of novel anticancer drugs due to their essential role in mitosis and cell division.<sup>1</sup> The microtubule targeting drugs such as vincristine, colchicine, and taxanes, exert their effect on cell proliferation by inhibiting the microtubule, inducing cell cycle arrest in the G2-M phase and abnormal mitotic spindles.<sup>2</sup> Podophyllotoxin is the principal active compound isolated from Podophyllin, a resin obtained from *Podophyllum peltatum*, *Podophyllum emodi* and others (Fig. 1).<sup>3</sup> It is known as a strong microtubule destabilizing agent that binds to the colchicine site of tubulin, thus causing tubulin polymerization inhibition, and microtubule formation suppression.<sup>4,5</sup> Moreover, podophyllotoxin derivatives possess cathartic, antirheumatic, antiviral and antitumor properties.<sup>6–8</sup> Among podophyllotoxin analogues, 4-aza-podophyllotoxins have attracted considerable attention in anticancer drug discovery,<sup>9–14</sup> owing to their important biological activities in cell cycle arrest in the G2/M phase,<sup>15,16</sup> and caspase-3 dependent

apoptosis,<sup>17</sup> and as tubulin assembly inhibitors,<sup>17</sup> vascular-disrupting agents,<sup>18</sup> antitumor agents,<sup>19</sup> and insecticides (larvicidal).<sup>20</sup> The  $\gamma$ -butyrolactone ring D of 4-azapodophyllotoxins has played a vital role in the biological activities through binding to tubulin,<sup>21</sup> and its modifications caused a decrease of cytotoxicity in the derivatives.<sup>7,21–23</sup> The 3,4,5-trimethoxy substitutions of the E-ring generally resulted in an improvement in cytotoxicity.<sup>9</sup>

On the other hand, the nitrogen heterocyclic compounds have attracted the interest of scientists due to their bioactive properties.<sup>24–32</sup> Aza-anthraquinones, which are crucial analogues of 1,4-naphthoquinones, have known as intercalating DNA binding agents in cancer chemotherapy due to the planar structure (Fig. 1).<sup>33,34</sup> Besides that, aza-anthraquinone derivatives have exhibited significant antimicrobial, antioxidant, anti-inflammatory and cytotoxic effect.<sup>35–38</sup> The quinonoid moiety produces reactive oxygen species (ROS) resulting in oxidative stress,<sup>39,40</sup> stimulates a free radical mechanism that leads to cancer cell destruction,<sup>41</sup> and serves as an electrophile that reacts with different nucleophiles present in biological systems.<sup>40,42</sup> Although several hybrids of podophyllotoxin have been reported in literature, such as podophyllotoxin piperazine acetate ester derivatives,<sup>43</sup> podophyllotoxin-norcantharidin,<sup>44</sup> and quinazolino linked 4 $\beta$ -amidopodophyllotoxins,<sup>45</sup> there has been no study of the synthesis of podophyllotoxin-azaanthraquinone hybrids bearing  $\gamma$ -butyrolactone ring as well as assessment of cytotoxicity profile of these hybrids. Thus, in the view of pharmaceutical importance of pharmacophoric 4-aza-podophyllotoxin and aza-anthraquinone, in our previous study,<sup>46</sup> novel podophyllotoxin-naphthoquinone compounds as potent anti-cancer agents were synthesized *via*

<sup>a</sup>Graduate University of Science and Technology, Vietnam Academy of Science and Technology (VAST), 18 Hoang Quoc Viet, Cau Giay, Hanoi, Vietnam. E-mail: ngvtuyen@hotmail.com; ngvtuyen@ich.vast.vn

<sup>b</sup>Institute of Chemistry, Vietnam Academy of Science and Technology (VAST), 18 Hoang Quoc Viet, Cau Giay, Hanoi, Vietnam. E-mail: hathanhnguyen1512@gmail.com

<sup>c</sup>Hanoi University of Pharmacy, 13-15 Le Thanh Tong, Hoan Kiem, Hanoi, Vietnam

† Electronic supplementary information (ESI) available. See <https://doi.org/10.1039/d2ra03312g>



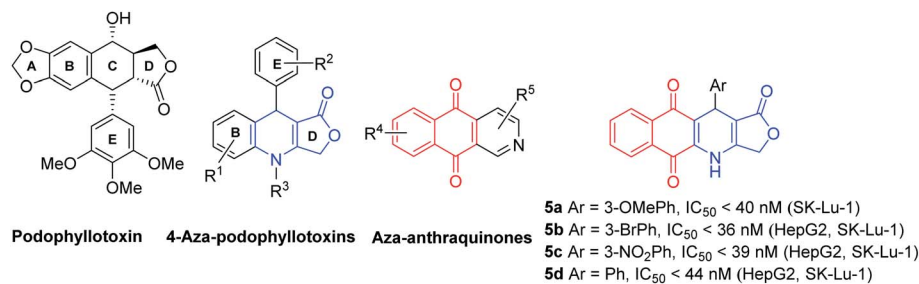


Fig. 1 Structure of podophyllotoxin derivatives, aza-anthraquinones derivatives and podophyllotoxin-naphthoquinone compounds (5a, 5d).

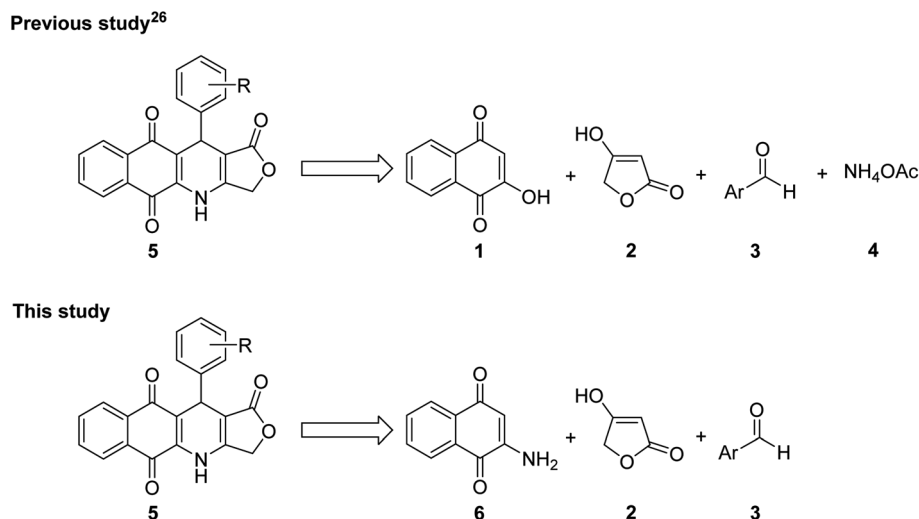


Fig. 2 Design strategy for the potent cytotoxic podophyllotoxin-naphthoquinone compounds.

microwave-assisted four-component reactions of 2-hydroxy-1,4-naphthoquinone (1), tetronic acid (2), aromatic aldehydes 3, and ammonium acetate (4) in glacial acetic acid (Fig. 2). Although this is a promising approach, it has the limitation of not being able to synthesize several podophyllotoxin-naphthoquinone compounds, for example, derivatives bearing hydroxy, trimethoxy, dimethoxy or heterocyclic substituents on aryl moiety.

Accordingly, with the aim to discover more potent cytotoxic podophyllotoxin-naphthoquinones, in this study, we have reported a new, simple and more efficient method for the synthesis of potent cytotoxic compounds 5a–g and their new derivatives *via* microwave-assisted three-component reactions (Fig. 2), together with evaluation of their cytotoxic activity against several cancer cell lines. Moreover, in an effort to investigate more clearly the mechanism of action of the highly potent cytotoxic compounds, herein, *in vitro* biological activities of two compounds 5a, and 5b on cell cycle progression, apoptosis, and molecular docking experiments were explored.

## Results and discussion

### Chemistry

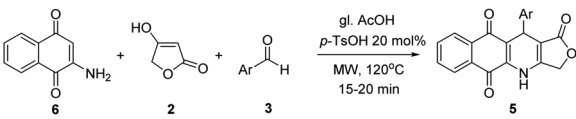
Compounds 5 were synthesized efficiently *via* microwave-assisted three-component reactions of 2-amino-1,4-naphthoquinone (6),

tetronic acid (2), and (hetero)aromatic aldehydes 3 in glacial acetic acid (gl. AcOH) as a solvent and *p*-toluenesulfonic acid (*p*-TsOH, 20 mol%) as a catalyst (Table 1). Notably, in comparison with the method reported in the previous study, this new strategy provided compounds 5a–g in higher yield and shorter reaction time. Moreover, it is important to mention that the substituents at the aromatic ring of the aldehyde component had no significant effect on the yield of these microwave-assisted three-component reactions. The structure of these compounds was fully characterized by IR, <sup>1</sup>H and <sup>13</sup>C NMR, and HRMS, which were provided in the Experimental section.

A possible mechanistic interpretation of these three-component reactions begun with the Knoevenagel condensation of 2-amino-1,4-naphthoquinone (6) with (hetero)aromatic aldehydes, followed by spontaneous dehydration to afford intermediates 10. The intermediates 10 underwent the Michael addition, intramolecular cyclization and dehydration sequence of steps to furnish the final products 5 (Scheme 1).

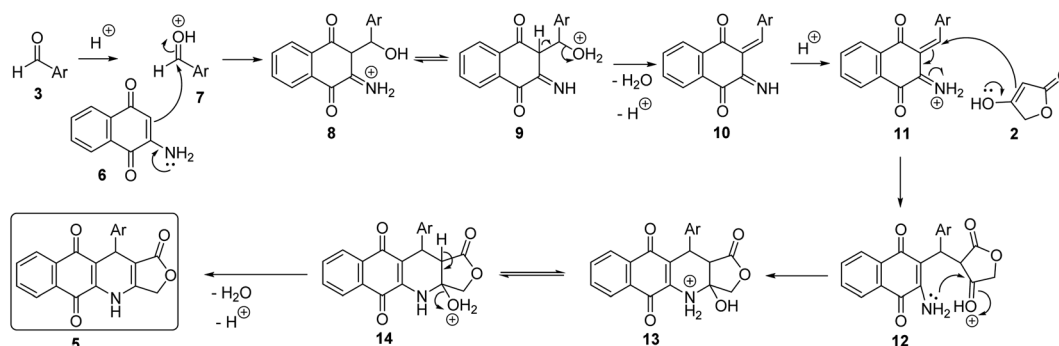
### Cytotoxicity of new podophyllotoxin-naphthoquinone derivatives

The new podophyllotoxin-naphthoquinone compounds 5g–o were evaluated for their cytotoxicity against 4 human cancer cell lines (KB, HepG2, MCF7, A459). Ellipticine was used as positive

Table 1 Synthesis of podophyllotoxin-naphthoquinone compounds *via* microwave-assisted three-component reactions<sup>a</sup>


Entry	Product	Ar	Time (min)	Yield <sup>b</sup> (%)	Mp <sup>c</sup> (°C)
1	5a	3-OMePh	15	86	290–293 <sup>d</sup>
2	5b	3-BrPh	15	83	328–329 <sup>d</sup>
3	5c	3-NO <sub>2</sub> Ph	15	75	283–285 <sup>d</sup>
4	5d	Ph	15	84	329–334 <sup>d</sup>
5	5e	4-MePh	15	88	320–322 <sup>d</sup>
6	5f	2-NO <sub>2</sub> Ph	15	73	289–292 <sup>d</sup>
7	5g	3-Oxo-1,3-dihydro benzofuran-5-yl	15	85	295–296 <sup>d</sup>
8	5h	2-OHPh	20	80	311–312
9	5i	4-OHPh	20	79	304–305
10	5j	4-NO <sub>2</sub> Ph	15	82	298–299
11	5k	4-CNPh	15	89	306–307
12	5l	3,4-(MeO) <sub>2</sub> Ph	15	85	288–289
13	5m	3,4,5-(MeO) <sub>3</sub> Ph	15	86	310–311
14	5n	Pyridin-3-yl	15	81	210–212
15	5o	5-Br-pyridin-2-yl	15	83	274–275

<sup>a</sup> All the reactions were carried out in 1 mmol scale in 3 mL solvent at 120 °C under MW at the maximum power of 150 W, and the ratio of 6/2/3 was 1/1/1. <sup>b</sup> Isolated yields. <sup>c</sup> Decomposed. <sup>d</sup> These results were reported in our previous study.<sup>46</sup>



Scheme 1 Plausible mechanism for the synthesis of podophyllotoxin-naphthoquinone compounds 5.

control. As shown in Table 2, compound 5m with Ar = 3,4,5-trimethoxyphenyl (entry 13) and compounds 5a–d (entries 1–4) were found to be highly potent cytotoxic agents against human cancer cell lines. However, compound 5m exhibited strong toxic activity against non-cancerous human embryonic kidney (Hek-293) cell line with IC<sub>50</sub> value of 0.03 μM. Compounds 5a and 5b showed lower toxic to the Hek-293 with IC<sub>50</sub> values of 9.35 and 7.20 μM, respectively. Therefore, the most potent compounds 5a and 5b were investigated further to assess their ability to influence cell cycle progression and apoptosis in SK-Lu-1 cells. Based on the results reported in the previous study<sup>46</sup> and this study, preliminary investigation of the structure–activity relationships (SARs) of products revealed that the electronic nature of substituents on aryl group had no significant effect on the cytotoxicity of these products. However, single substitutions at C2 or C4 positions of aryl moiety generally led to diminished cytotoxicity.

### Compounds 5a, 5b induced cell cycle G2/M phase arrest in SK-LU-1 cells

Cell cycle progression is a tightly regulated process connected with proliferation and differentiation.<sup>47</sup> Most of the microtubule destabilizing compounds induce mitotic arrest at the G2/M phase of cell cycle progression.<sup>48</sup> Toward this, as compounds 5a, 5b exhibited anti-proliferative efficacy on human lung SK-LU-1 cancer cells, their influence on the cell cycle progression has been assessed by monitoring the distribution of cells in populations based on distinct phases including G0/G1 phase, S phase (Synthesis), and G2/M phase (Gap 2/Mitosis). Ellipticine<sup>49–51</sup> and Vincristine,<sup>2</sup> which are anticancer agents currently in clinical use for the treatment of various diseases, were used as positive controls.

As depicted in the Fig. 3 and Table 3, both tested compounds suppressed a G2/M arrest in SK-LU-1 cells in dose-dependent manner. Treatment with compounds 5a, 5b at 0.16 μM and 0.32



Table 2 Cytotoxicity of the synthesized compounds against KB, HepG2, MCF7, A549, SK-LU-1, and Hek-293 cell lines

Entry	Comp	IC <sub>50</sub> (μM)					
		KB	HepG2	MCF7	A549	SK-Lu-1	Hek-293
1 <sup>a</sup>	5a	1.23 ± 0.01	0.46 ± 0.01	>2.5	NA <sup>b</sup>	<0.040	9.35 ± 0.44
2 <sup>a</sup>	5b	1.71 ± 0.07	<0.036	>2.5	NA <sup>b</sup>	<0.036	7.20 ± 0.05
3 <sup>a</sup>	5c	1.16 ± 0.01	<0.039	2.19 ± 0.02	NA <sup>b</sup>	<0.039	1.47 ± 0.04
4 <sup>a</sup>	5d	1.54 ± 0.01	<0.044	1.98 ± 0.04	NA <sup>b</sup>	<0.044	1.34 ± 0.01
5 <sup>a</sup>	5e	>2.50	2.24 ± 0.01	>2.50	NA <sup>b</sup>	1.65 ± 0.03	>20
6 <sup>a</sup>	5f	1.86 ± 0.02	0.47 ± 0.01	>2.50	NA <sup>b</sup>	0.08 ± 0.01	4.78 ± 0.14
7 <sup>a</sup>	5g	2.34 ± 0.26	>2.50	>2.50	NA <sup>b</sup>	2.22 ± 0.04	9.95 ± 0.01
8	5h	0.57 ± 0.02	0.63 ± 0.02	1.61 ± 0.03	0.43 ± 0.01	NA	2.03 ± 0.06
9	5i	>2.50	>2.50	2.23 ± 0.06	1.59 ± 0.03	NA	6.46 ± 0.15
10	5j	>2.50	>2.50	>2.50	1.12 ± 0.04	NA	7.17 ± 0.16
11	5k	>2.50	>2.50	>2.50	2.03 ± 0.05	NA	>20
12	5l	0.52 ± 0.02	0.53 ± 0.02	2.28 ± 0.07	1.10 ± 0.02	NA	2.23 ± 0.08
13	5m	0.02 ± 0.01	0.02 ± 0.01	0.12 ± 0.03	0.62 ± 0.02	NA	0.03 ± 0.01
14	5n	0.62 ± 0.01	>2.50	1.96 ± 0.04	0.61 ± 0.02	NA	1.81 ± 0.05
15	5o	>2.50	>2.50	>2.50	>2.50	NA	>20
16	Ellipticine	1.15 ± 0.01	1.51 ± 0.05	1.82 ± 0.03	1.60 ± 0.02	NA	6.18 ± 0.11

<sup>a</sup> These results were reported in our previous study.<sup>46</sup> <sup>b</sup> NA: not analyzed.

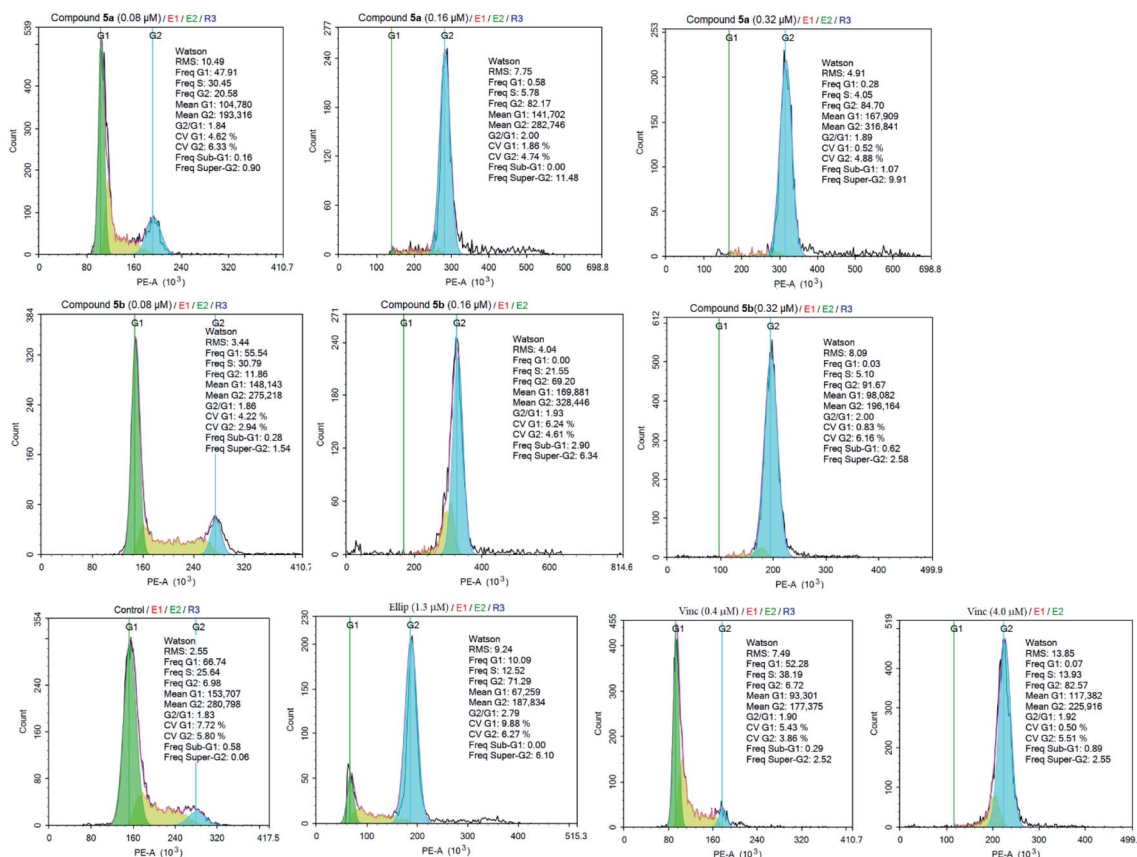


Fig. 3 Effect of compounds 5a, 5b on cell cycle distribution in SK-LU-1 cells. Cells were treated with tested samples, DMSO 0.05% (negative reference) and positive controls including Ellipticine (1.3 μM), Vincristine (0.4 μM and 4 μM) for 24 h. Cell cycle distribution was evaluated by flow cytometry Novocyte (ACEA Biosciences, San Diego, CA, USA).

μM caused a significant rise of cell accumulation in G2/M phase, accompanied by a strong decrease of cells in G1 phase and S phase. These results suggested that tested compounds possessed

anti-proliferative activity through concentration-dependently inducing a significant G2/M-phase arrest, which was a representative feature shared by tubulin polymerization inhibitors.<sup>48,52</sup>



**Table 3** Percentage of cell by phases of tested compounds in SK-LU-1 cells

Sample	Percentage of cell by phases (%)		
	% G0/G1	% S	% G2/M
5a (0.08 $\mu$ M)	47.91	30.45	20.58
5a (0.16 $\mu$ M)	0.58	5.78	82.17
5a (0.32 $\mu$ M)	0.28	4.05	84.70
5b (0.08 $\mu$ M)	55.54	30.79	11.86
5b (0.16 $\mu$ M)	0.00	21.55	69.20
5b (0.32 $\mu$ M)	0.03	5.10	91.67
Control	66.74	25.64	6.98
Ellipticine (1.3 $\mu$ M)	10.09	12.52	71.29
Vincristine (0.4 $\mu$ M)	52.28	38.19	6.72
Vincristine (4.0 $\mu$ M)	0.07	13.93	82.57

### Compounds 5a, 5b induced apoptosis in SK-LU-1 cells

Mitotic arrest of tumor cells by tubulin-targeted agents is generally associated with cellular apoptosis. As compounds **5a**, **5b** could effectively cause G2/M-phase arrest, the different flow cytometry-based assays, namely, assay of morphology, assay of caspase-3/7 enzymatic activities, and assay of immunophenotyping have been used to assess the effect of compounds **5a**, **5b** on apoptosis, a well-known programmed cell death mechanism.<sup>53</sup>

### Assay of morphology

Staining cells with Hoechst stain, an excellent probe to distinguish live, necrotic, early- and late-apoptotic cells, has been used to make the morphology of cell treated with compound **5a**, **5b** readily visible by fluorescence microscopy.<sup>54</sup> Whereas the nuclei of healthy cells are generally spherical, and the DNA is evenly distributed, the apoptotic cells are defined by chromatin condensation and nuclear fragmentation.<sup>55,56</sup> As shown in Fig. 4, the photomicrograph of apoptotic changes in LU-1 cells treated with the tested compounds displayed nuclei predominantly fragmented, and stained more intensely because of chromatin condensation. These results revealed that compounds **5a**, **5b** induced significant changes in cell morphology including nucleus fragmentation and chromatin condensation, which are hallmarks of apoptosis in the nucleus.<sup>55,56</sup>

### Assay of caspase-3/7 enzymatic activities

Caspase-3/7, executioner members of caspase family, are essential for cellular apoptotic authentication because their substrates can regulate the key morphological changes in apoptosis such as DNA degradation, chromatin condensation, and membrane blebbing.<sup>57</sup> They are the essential marker to assess the apoptotic inductive activities of tested compounds. Because compounds **5a**, **5b** caused nucleus fragmentation and

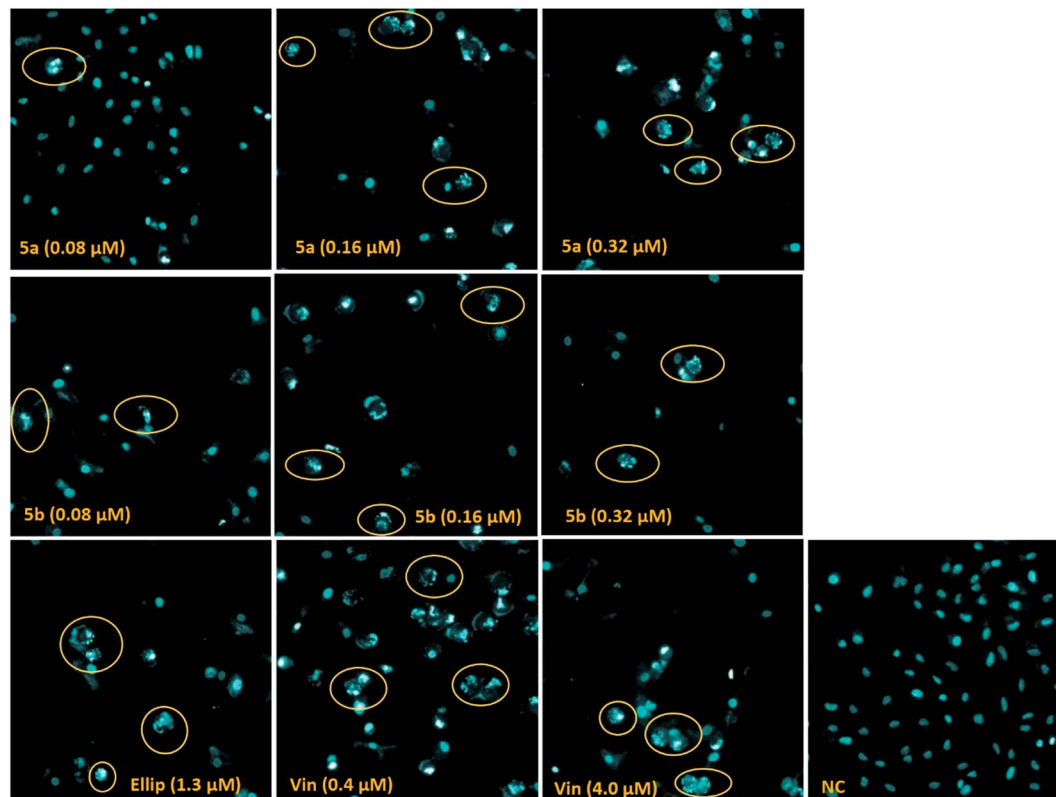


**Fig. 4** Photomicrograph of apoptotic changes in LU-1 cells treated with compounds **5a**, **5b** at 0.08  $\mu$ M, 0.16  $\mu$ M, and 0.32  $\mu$ M; negative control (NG); Ellipticine (Ellip) at 1.3  $\mu$ M; Vincristine (Vin) at 0.4  $\mu$ M and 4.0  $\mu$ M. Cells were stained with Hoechst and then observed by fluorescence microscopy. Some cells with fragmented nuclei are enclosed within circles.





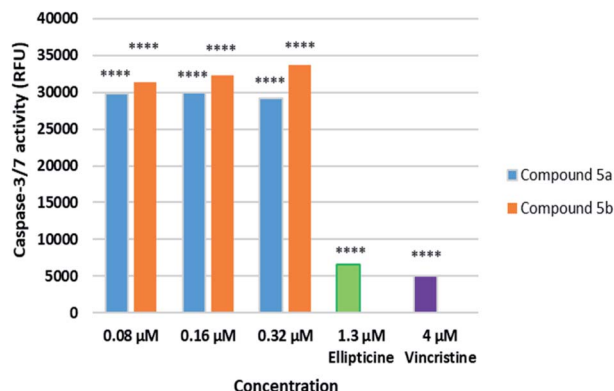


**Fig. 5** Effect of compounds **5a**, **5b** on caspase-3/7 activity. Cells were treated with different concentrations of compound **5a**, **5b**, Ellipticine (1.3 μM), and Vincristine (4 μM), followed by harvesting and mixing with Apo-ONE® Caspase-3/7 reagent. A Tecan GENios Pro microplate reader was used to determine relative fluorescence units (RFU), directly proportional to the activation of caspase-3/7. Caspase activity = RFU value of tested sample – RFU value of the blank.

chromatin condensation, the effect of compounds **5a**, **5b** on caspase 3/7 activation in SK-LU-1 human cancer cells was subsequently evaluated at different concentration of 0.08 μM,

0.16 μM, and 0.32 μM (Fig. 5) and compared to Ellipticine. The results indicated that treatment with compounds **5a**, **5b** at different concentration resulted in significant increases in caspase activity. Noticeably, these compounds enhanced 4-5-fold caspase-3/7 activity as compared to Ellipticine (1.3 μM). It was worth noting that compound **5a**, **5b** activated the caspase pathway, which trigger apoptosis of SK-LU-1 human cancer cells and suppress cell proliferation.<sup>52,58</sup>

### Assay of immunophenotyping

In the flow cytometric immunophenotyping method, annexin V labeled with a fluorophore or biotin can identify apoptotic cells by binding to phosphatidylserine (PS) exposed on the outer leaflet of their plasma membrane.<sup>59–61</sup> Thus, this method has allowed the detection of the effect of compounds **5a**, **5b** at different concentrations on the proportion of apoptotic cells in SK-LU-1 human cancer cells. As described in Fig. 6, and Table 4, both compounds **5a**, **5b** caused a dose-dependent increase in the percentage of apoptotic cells. Taken compound **5b** as an example, the cells treated with compounds **5b** at concentrations of 0.08 μM, 0.16 μM, and 0.32 μM led to an accumulation of apoptotic cells from 1.96% (control) to 8.04%, 11.87%, and 21.10%, respectively. A small percentage of cells, which died *via*

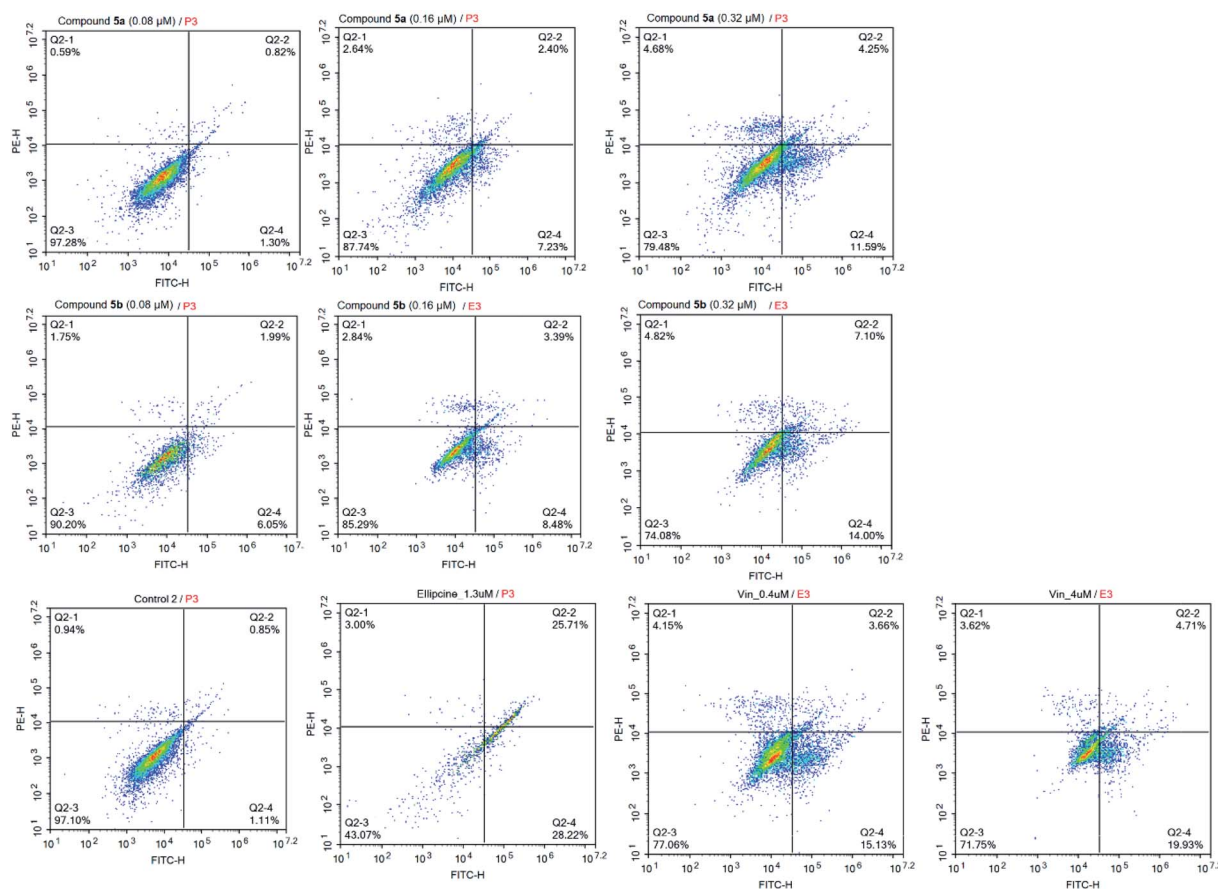


**Fig. 6** Analyses of apoptosis induction in SK-LU-1 cells. Detection of apoptotic cells after Annexin-V/PI staining by flow cytometry. Cells were treated with different concentrations of compound **5a**, **5b**, control, and references, followed by harvesting and staining with Annexin-V/PI for 24 hours. The diverse cell stages were given as live (Q3), early apoptotic (Q4), late apoptotic (Q2), and necrotic cells (Q1).



Table 4 Percentage of apoptosis

Sample	% Necrotic cells	% Early apoptosis cells	% Late apoptosis cells	% Total apoptosis cells
5a (0.08 $\mu$ M)	0.59	1.30	0.82	2.12
5a (0.16 $\mu$ M)	2.64	7.23	2.40	9.63
5a (0.32 $\mu$ M)	4.68	11.59	4.25	15.84
5b (0.08 $\mu$ M)	1.75	6.05	1.99	8.04
5b (0.16 $\mu$ M)	2.84	8.48	3.39	11.87
5b (0.32 $\mu$ M)	4.82	14.00	7.10	21.10
Control	0.94	1.11	0.85	1.96
Ellipticine (1.3 $\mu$ M)	3.00	28.22	25.71	53.93
Vincristine (0.4 $\mu$ M)	4.15	15.13	3.66	18.79
Vincristine (4.0 $\mu$ M)	3.62	19.93	4.71	24.64

the necrotic pathway, could be dead cells in the late stages of apoptosis presenting necrotic features due to a process called “apoptotic necrosis” or “secondary necrosis”.<sup>62</sup> Hence, the results re-confirmed that the compounds **5a**, **5b** exhibited the anti-proliferative effect through dose-dependently triggering cellular apoptosis of SK-LU-1 cells, particularly in the early apoptotic stage.

### Molecular docking study

On the basis of biological assessments, it is of interest investigating the interactions between synthesized compounds against potential anticancer dual targets, including tubulin and procaspase. To do so, there are a lot of studies exploring docking and/or docking in combination of quantum-mechanical atomistic simulation, such as DFT method, and so on.<sup>63,64</sup>

In this study, as for screening, docking and scoring simulations therefore were preferably used. It is widely described in the literature the structures of tubulin as heterodimers repeatedly assembled by  $\alpha$ - and  $\beta$ -tubulin monomers with both size of  $\sim 50$  kDa and sequence homology of more than 40% identity.<sup>65,66</sup>

Tubulin inhibitory agents, such as colchicine, the vinca alkaloids, and maytansine, normally bind to the lateral contacts of adjacent  $\alpha\beta$ -subunits that promote loss of the microtubule assembly. According to Massaroti *et al.*, the colchicine-binding site (CBS) is a pocket composed of three zones (Fig. 7): (i) zone 1 located at the  $\alpha$ -subunit and encompassed by amino acids Asn101a, Ser178a, Val181a..., (ii) zone 2 is an accessory hydrophobic pocket mainly situated at  $\beta$ -subunit and surrounded by Cys241b, Leu248b, Ala250b, Leu255b, Ala316b, Lys352b, *etc.*, and (iii) zone 3 is buried deeper in the  $\beta$ -subunit formed by Ile4b, Asn167b, Phe169b, Tyr202b, Val238b among others.<sup>62</sup> Among them, zone 2 is recognized as the cavity to accommodate most of the structures of the ligands which normally possess at least two separated aromatic systems (Fig. 7).<sup>66</sup>

To validate the docking protocol, we firstly redocked colchicine in the CBS of the complex 4O2B and compared the binding modes with the co-crystal ligand. As the results, the redocked colchicine showed highly overlapped degree with the native ligand with the root-mean square deviation (RMSD) of 0.57 Å. The redocked interactions in the active site were also similar to the original ligand, including H-bonding between the

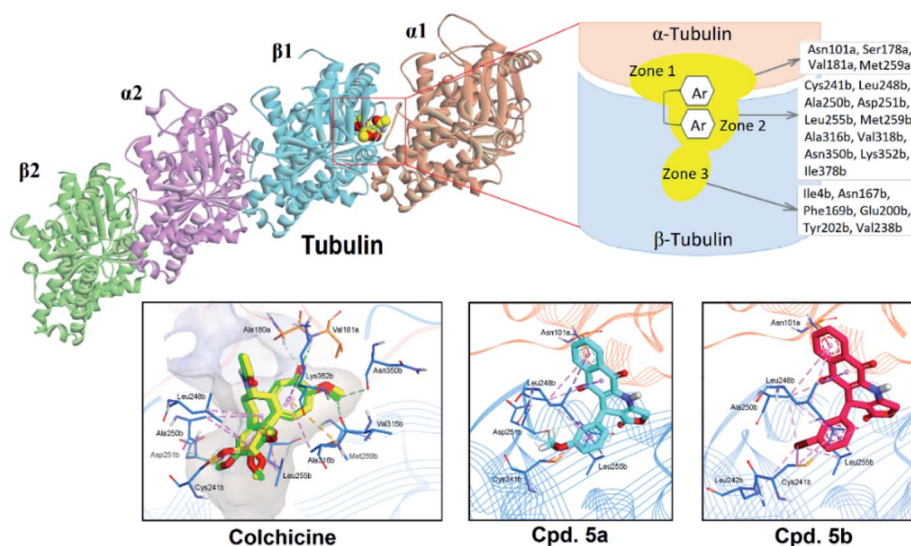


Fig. 7 The three-zone structure of colchicine-binding site (CBS) and docking interactions of colchicine, **5a** and **5b** with tubulin.



methoxytropone ring with Ala180a and Val181a of zone 1, hydrophobic interactions with Leu248b, Ala250b, Leu255b, Met259b and Ala316b of zone 2. The binding affinity of Colchicine was  $-9.4 \text{ kcal mol}^{-1}$ . The obtained results appropriately demonstrated the validity of the docking protocol applied. The next steps were to dock two compounds **5a**, **5b** into the CBS of tubulin. The results showed that pi-alkyl stacking was the main interactions between the ligands and target. In particular, both compounds formed multiple hydrophobic interactions with Cys241b, Leu248b, Ala250b, Leu255b of zone 2, and Asn101a of zone 1 (Fig. 7). It is also highlighted the role of C=O in the lactone ring that can create one H-bond with Leu255b. Our findings are also in agreement with other DFT and MEP mapping computations which demonstrated the role of electron-rich aromatic moiety for the protein's hydrogen-bonding interactions.<sup>64,67,68</sup> The binding affinities of **5a** and **5b** were  $-7.8$  and  $-7.1 \text{ kcal mol}^{-1}$  respectively. In summary, **5a** and **5b**, being classified as classical tubulin inhibitors, similarly interacted with residues at the zone 1 and 2 of CBS and provided lower affinity against tubulin target than colchicine.

Given the caspase activity of synthesized compounds, we desired to examine their procaspase activation through docking simulation. To do so, we selected a procaspase structure in complex with PAC-1 determined by Delgado and Hardy (PDB ID: 4FXO),<sup>69</sup> which contains the cofactor Zn in the active site for the docking studies. As widely described in the literature, active caspase-3/7 is a dimer of two cleaved procaspases and its catalytic activity, at the normal state, is inhibited by Zn. As can be observed in the crystal structure of 4FXO, Zn interacts with Lys36, Glu244, His287 and a water molecule.<sup>70</sup> To induce the procaspase activation, ligands must be able to form stable chelation with inhibitory Zn ion. By docking PAC-1 into the active site of procaspase, we revealed that this compound could active procaspase by chelating Zn *via* the key *ortho*-hydroxy *N*-acylhydrazone moiety (Fig. 8). This result is similar to that published previously.<sup>71,72</sup> We then continued docking **5a** and **5b**

into the allosteric site of the target, and compared their interactions with those obtained for PAC-1. As the results, **5a** and **5b** could form stable chelation with Zn ion *via* heteroatoms N and O of quinone moiety of the podophyllotoxin fragment. There is a difference between the coordination geometry between PAC-1 and **5a**, **5b** as shown in Fig. 8. However, as a limitation of this study, electronic and intramolecular surface characteristics have could not analyzed by using docking assays. It is recommended to carry out in the future studies quantum-mechanical atomistic simulation, such as DFT method.<sup>73,74</sup> The GBVI/WSA binding free energy calculated for PAC-1 was  $-6.59 \text{ kcal mol}^{-1}$ , which is lower than **5a** ( $-7.19 \text{ kcal mol}^{-1}$ ) and similar to that of **5b** ( $-6.70 \text{ kcal mol}^{-1}$ ).

### Computational ADMET prediction

It is desired to examine the drug-like characteristics of bioactive compounds by analyzing physicochemical and ADMET related properties. To do so, ADMETlab 2.0 tool was effectively used to calculate number of physicochemical properties and ADMET endpoints.<sup>75</sup> Fig. 9 showed the computed 13 properties and their drug-like ranges (upper and lower limits). It can be seen in Fig. 9 that almost all physicochemical properties of **5a** and **5b** fall within the optimal range except their lipophilicity characterized by both the partition coefficient ( $\log P$ ) and the physiological pH-based distribution coefficient ( $\log D$ , pH = 7.4). This could be the main drawback of the current podophyllotoxin derivatives in order to develop an oral drug-like candidate.<sup>70</sup>

This fact was then confirmed by using the 3PRule and the Provisional Biopharmaceutical Classification Systems (PBCS) developed by Pham-The *et al.*<sup>76,77</sup> Accordingly, **5a** and **5b** were predicted to have moderate-to-low permeability through the gastrointestinal epithelial membrane (Caco-2) with an oral fraction absorbed lower than 30%. By computing the bioavailability score defined by Martin,<sup>78</sup> these compounds were predicted to have similar intestinal absorption and oral

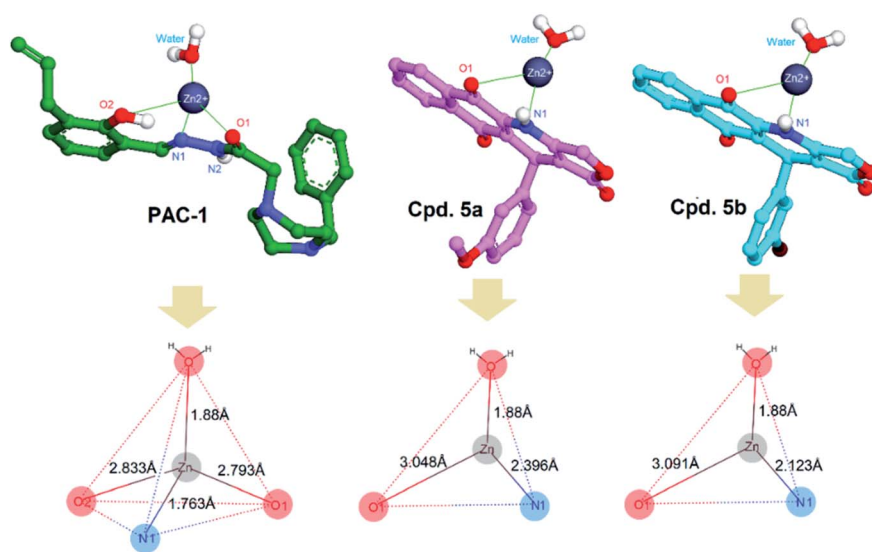


Fig. 8 Metal complex and geometries of PAC-1, **5a** and **5b** with Zn ion bound to the procaspase target (PDB ID: 4FXO).



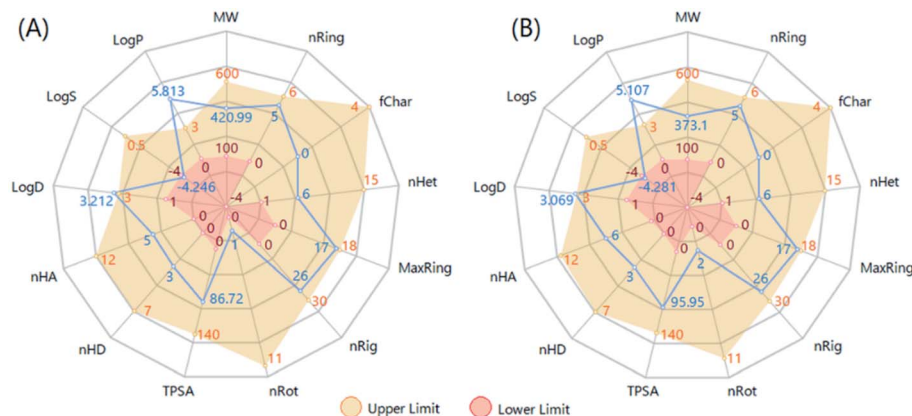


Fig. 9 Predicted physicochemical properties of **5a** (A) and **5b** (B) compared with drug optimal ranges. fChar: formal charge; log *D*, log of octanol partition coefficient at physiological pH 7.4; log *P*, log of octanol partition coefficient; log *S*, log of aqueous solubility ( $\text{mol L}^{-1}$ ); MaxRing, number of atoms in the biggest ring; MW, molecular weight; nHA, number of hydrogen bond acceptors; nHD, number of hydrogen bond donors; nHet, number of heteroatoms; nRig, number of rigid bonds; nRing, number of rings; nRot, number of rotatable bonds; TPSA, topological polar surface area ( $\text{\AA}^2$ ).

bioavailability with a score of 0.55. The main hepatic metabolism-limiting pathway was through CYP2D6 and CYP3A4. These compounds, therefore, did not accomplish the Lipinski's Ro5. In addition, these compounds displayed no interaction with the efflux P-gp pump, which is responsible for multi-drug resistance including many chemotherapeutic drugs.<sup>76</sup> Another important drug-drug interaction includes the inhibitory effect against hERG (the human Ether-à-go-go-Related Gene), which is associated with fatal cardiac adverse reaction.<sup>79</sup> Our calculation showed no interaction between **5a**, **5b** and this channel. Overall, the current ADMET estimation for **5a** and **5b** highlighted the limitation of absorption profile *via* the oral administration due to their excessive lipophilicity.

## Experimental

### General considerations

All chemicals and solvents, purchased from Aldrich or Merck, were used directly as purchased unless otherwise noted. The chemicals have a guaranteed purity of  $\geq 97\%$ . Anton Paar Microwave Synthetic Reactor Monowave 400 was used for microwave synthesis. The progress of reaction was checked by using TLC Silica gel 60 F<sub>254</sub> and UV light at 254 nm. Merck silica gel 60 (240–400 mesh) was used for column flash chromatography to purify the products. Melting points were identified by using a Büchi Melting Point B-545 and were uncorrected. IR analysis was recorded on PerkinElmer Spectrum Two spectrometer in KBr pellet, a Bruker Avance III spectrometer (600 and 150 MHz) and an SCIEX X500 QTOF mass spectrometer were used to record IR spectra, nuclear magnetic resonance spectra and HRMS, respectively.

Hoechst 33342 bought from Sigma was dissolved in DMSO at concentration of  $10 \text{ mg mL}^{-1}$  and then stored at  $-20^\circ \text{C}$  in a dark place. Kit Annexin V and PI/dead cell apoptosis® from Invitrogen. Kit ApoONE® Homogeneous Caspase-3/7 was bought from Promega, USA. Ellipticine was used as references.

Inverted microscope Zeiss, fluorescence microscope Olympus Ex 350 nm/Em 460 nm, spectrophotometer Biotek, spectrofluorometer Tecan GENios Pro Ex 485 nm/Em 530 nm, Novocyte flow cytometry (ACEA Biosciences, San Diego, CA, USA) with data analyzed & reported by ACEA's NovoExpress software were used for apoptosis analysis.

### General procedure for the synthesis of compounds **5**

The reaction of 2-amino-1,4-naphthoquinone **6** (1 mmol), tetronic acid **2** (1 mmol), aromatic aldehyde **3** (1 mmol), and *p*-TsOH (0.02 mmol) in glacial acetic acid (3 mL) was performed under microwave irradiation (150 W) at  $120^\circ \text{C}$  in 15–20 min. The reaction mixture was cooled to room temperature, added 20 mL of water, extracted with dichloromethane ( $3 \times 20 \text{ mL}$ ), washed with brine ( $3 \times 10 \text{ mL}$ ), dried over sodium sulfate, and the solvent removed by vacuum. The crude products **5** were then purified by column chromatography using a *n*-heptane-ethyl acetate eluent (6 : 4, v/v).

**11-(3-Methoxyphenyl)-4,11-dihydrobenzo[*g*]furo[3,4-*b*]quinoline-1,5,10(3*H*)-trione (5a).** Red solid; yield: 321 mg (86%). <sup>1</sup>H NMR (DMSO-*d*<sub>6</sub>, 600 MHz):  $\delta$  = 10.61 (s, 1H, NH), 8.06 (dd, 1H, *J* = 1.20, 7.8 Hz), 7.90 (dd, 1H, *J* = 1.8, 7.8 Hz), 7.84 (td, 1H, *J* = 1.2, 7.2 Hz), 7.81 (td, 1H, *J* = 1.2, 7.2 Hz), 7.17 (t, 1H, *J* = 8.4 Hz), 6.87 (d, 1H, *J* = 7.8 Hz), 6.85 (t, 1H, *J* = 2.4 Hz), 6.74 (dd, 1H, *J* = 2.4, 7.8 Hz), 4.98 (d, 1H, *J* = 16.8 Hz), 4.98 (s, 1H), 4.88 (dd, 1H, *J* = 1.2, 16.8 Hz), 3.69 (s, 3H, OCH<sub>3</sub>), lit.<sup>46</sup>

**11-(3-Nitrophenyl)-4,11-dihydrobenzo[*g*]furo[3,4-*b*]quinoline-1,5,10(3*H*)-trione (5b).** Violet solid; yield: 322 mg (83%). <sup>1</sup>H NMR (DMSO-*d*<sub>6</sub>, 600 MHz):  $\delta$  = 10.66 (s, 1H, NH), 8.07 (dd, 1H, *J* = 1.8, 7.2 Hz), 7.90 (dd, 1H, *J* = 1.8, 7.2 Hz), 7.84 (td, 1H, *J* = 1.8, 7.2 Hz), 7.81 (td, 1H, *J* = 1.8, 7.2 Hz), 7.52 (t, 1H, *J* = 1.8 Hz), 7.38–7.34 (m, 2H), 7.23 (t, 1H, *J* = 7.8 Hz), 5.02 (s, 1H, H-11), 5.00 (d, 1H, *J* = 16.8 Hz), 4.90 (d, 1H, *J* = 1.2, 16.8 Hz), lit.<sup>46</sup>

**11-(3-Bromophenyl)-4,11-dihydrobenzo[*g*]furo[3,4-*b*]quinoline-1,5,10(3*H*)-trione (5c).** Red solid; yield: 317 mg (75%). <sup>1</sup>H NMR (DMSO-*d*<sub>6</sub>, 600 MHz):  $\delta$  = 10.74 (s, 1H, NH), 8.17 (t, 1H, *J* =



1.8 Hz), 8.07 (dd, 1H,  $J = 1.8, 6.6$  Hz), 8.06–8.03 (m, 1H), 7.89–7.88 (m, 1H), 7.85–7.80 (m, 3H), 7.57 (t, 1H,  $J = 8.4$  Hz), 5.22 (s, 1H, H-11), 5.01 (d, 1H,  $J = 16.8$  Hz), 4.93 (dd, 1H,  $J = 0.6, 16.8$  Hz), lit.<sup>46</sup>

**11-(Phenyl)-4,11-dihydrobenzo[*g*]furo[3,4-*b*]quinoline-1,5,10(3*H*)-trione (5d).** Red solid; yield: 288 mg (84%). <sup>1</sup>H NMR (DMSO-*d*<sub>6</sub>, 500 MHz):  $\delta = 10.63$  (s, 1H, NH), 8.06 (d, 1H,  $J = 7.0$  Hz), 7.88 (d, 1H,  $J = 7.5$  Hz), 7.81 (quint, 2H,  $J = 7.0$  Hz), 7.32 (d, 2H,  $J = 7.5$  Hz), 7.26 (t, 2H,  $J = 7.5$  Hz), 7.15 (t, 1H,  $J = 7.5$  Hz), 5.00 (s, 1H), 4.98 (d, 1H,  $J = 16.5$  Hz), 4.89 (d, 1H,  $J = 16.5$  Hz), lit.<sup>46</sup>

**11-(2-Hydroxyphenyl)-4,11-dihydrobenzo[*g*]furo[3,4-*b*]quinoline-1,5,10(3*H*)-trione (5h).** Red orange solid; yield: 287 mg (80%); mp 311–312 °C with decomp. IR (KBr)  $\nu_{\text{max}}/\text{cm}^{-1}$  3117, 2920, 2850, 1723, 1661, 1584, 1508, 1401, 1354, 1337, 1305, 1275, 1250, 1203, 1166, 1134, 1072, 1017, 925, 867, 758, 719, 697. <sup>1</sup>H NMR (DMSO-*d*<sub>6</sub>, 600 MHz):  $\delta = 10.52$  (s, 1H, NH), 9.30 (s, 1H, OH), 8.04 (dd, 1H,  $J = 0.6, 7.8$  Hz), 7.86 (dd, 1H,  $J = 0.6, 7.8$  Hz), 7.82 (td, 1H,  $J = 1.2, 7.2$  Hz), 7.78 (td, 1H,  $J = 1.2, 7.2$  Hz), 7.14 (dd, 1H,  $J = 1.2, 7.8$  Hz), 6.96 (td, 1H,  $J = 1.2, 7.8$  Hz), 6.70–6.66 (m, 2H), 5.20 (s, 1H), 4.87 (t, 2H,  $J = 16.8$  Hz). <sup>13</sup>C NMR (DMSO-*d*<sub>6</sub>, 150 MHz):  $\delta = 182.03, 179.81, 171.16, 156.12, 154.97, 139.65, 134.94, 133.27, 131.90, 130.56, 130.49, 130.00, 127.71, 125.87, 125.70, 118.87, 118.74, 115.72, 101.35, 65.84, 30.68$ . HRMS  $m/z$  [ $M + \text{Na}$ ]<sup>+</sup> calcd for C<sub>21</sub>H<sub>13</sub>NNaO<sub>5</sub><sup>+</sup>: 382.0686; found: 382.0671.

**11-(4-Hydroxyphenyl)-4,11-dihydrobenzo[*g*]furo[3,4-*b*]quinoline-1,5,10(3*H*)-trione (5i).** Orange red solid; yield: 284 mg (79%); mp 304–305 °C with decomp. IR (KBr)  $\nu_{\text{max}}/\text{cm}^{-1}$  3227, 2932, 1726, 1663, 1595, 1493, 1473, 1398, 1351, 1334, 1300, 1245, 1195, 1160, 1135, 1074, 1015, 927, 803, 788, 724, 693, 669, 606, 584. <sup>1</sup>H NMR (DMSO-*d*<sub>6</sub>, 600 MHz):  $\delta = 11.39$  (s, 1H, NH), 10.08 (s, 1H, OH), 8.87 (d, 1H,  $J = 7.2$  Hz), 8.71 (d, 1H,  $J = 7.2$  Hz), 8.66 (t, 1H,  $J = 7.2$  Hz), 8.60 (t, 1H,  $J = 7.2$  Hz), 7.91 (d, 2H,  $J = 8.4$  Hz), 7.46 (d, 2H,  $J = 8.4$  Hz), 5.79 (d, 1H,  $J = 16.8$  Hz), 5.70 (s, 1H), 5.70 (d, 1H,  $J = 16.8$  Hz). <sup>13</sup>C NMR (DMSO-*d*<sub>6</sub>, 150 MHz):  $\delta = 182.15, 179.62, 171.19, 156.12, 155.58, 138.88, 135.17, 134.88, 133.32, 131.88, 130.16, 129.02, 128.00, 125.93, 125.72, 118.84, 114.93, 102.26, 65.98, 33.85, 30.65$ . HRMS (ESI<sup>+</sup>)  $m/z$  [ $M - \text{H}$ ]<sup>−</sup> calcd for C<sub>21</sub>H<sub>12</sub>NO<sub>5</sub><sup>−</sup>: 358.0720; found: 358.0618 (−28.9 ppm).

**11-(4-Nitrophenyl)-4,11-dihydrobenzo[*g*]furo[3,4-*b*]quinoline-1,5,10(3*H*)-trione (5j).** Orange red solid; yield: 318 mg (82%); mp 305–306 °C with decomp. IR (KBr)  $\nu_{\text{max}}/\text{cm}^{-1}$  3258, 3017, 2932, 1758, 1716, 1666, 1595, 1514, 1493, 1395, 1343, 1300, 1256, 1194, 1157, 1131, 1029, 1009, 933, 858, 834, 797, 726. <sup>1</sup>H NMR (DMSO-*d*<sub>6</sub>, 600 MHz):  $\delta = 10.74$  (s, 1H, NH), 8.14–8.11 (m, 2H), 8.09–8.06 (m, 1H), 7.87 (dd, 1H,  $J = 2.4, 6.6$  Hz), 7.86–7.80 (m, 2H), 7.67–7.63 (m, 2H), 5.18 (s, 1H), 4.98 (d, 1H,  $J = 16.8$  Hz), 4.92 (d, 1H,  $J = 1.2, 16.8$  Hz). <sup>13</sup>C NMR (DMSO-*d*<sub>6</sub>, 125 MHz):  $\delta = 182.02, 179.36, 170.93, 156.41, 151.29, 146.26, 140.06, 134.95, 133.48, 131.75, 130.30, 129.45$  (2C), 126.05, 125.76, 123.38 (2C), 117.20, 101.07, 66.25, 35.48. HRMS  $m/z$  [ $M - \text{H}$ ]<sup>−</sup> calcd for C<sub>21</sub>H<sub>11</sub>N<sub>2</sub>O<sub>6</sub><sup>−</sup>: 387.0622; found: 387.0513.

**4-(1,5,10-Trioxo-1,3,4,5,10,11-hexahydrobenzo[*g*]furo[3,4-*b*]quinolin-11-yl)benzonitrile (5k).** Orange solid; yield: 328 mg (89%); mp 306–307 °C with decomp. IR (KBr)  $\nu_{\text{max}}/\text{cm}^{-1}$  3449,

3291, 2227, 1775, 1755, 1665, 1594, 1498, 1438, 1395, 1335, 1299, 1194, 1160, 1134, 1110, 1022, 932, 843, 794, 724, 618. <sup>1</sup>H NMR (DMSO-*d*<sub>6</sub>, 600 MHz):  $\delta = 10.72$  (s, 1H, NH), 8.07 (dd, 1H,  $J = 1.8, 7.2$  Hz), 7.88 (dd, 1H,  $J = 1.2, 7.2$  Hz), 7.82 (double-quint, 2H,  $J = 1.8, 7.2$  Hz), 8.60 (t, 1H,  $J = 7.2$  Hz), 7.91 (d, 2H,  $J = 8.4$  Hz), 7.75–7.72 (m, 2H), 7.58–7.56 (m, 2H), 5.11 (s, 1H), 4.98 (d, 1H,  $J = 16.8$  Hz), 4.91 (dd, 1H,  $J = 1.2, 16.8$  Hz). <sup>13</sup>C NMR (DMSO-*d*<sub>6</sub>, 125 MHz):  $\delta = 182.10, 179.40, 171.05, 156.42, 149.42, 140.07, 134.99, 133.52, 132.24$  (2C), 131.80, 130.35, 129.26 (2C), 126.09, 125.81, 118.79, 117.28, 109.54, 101.20, 66.27, 35.63.

**11-(3,4-Dimethoxyphenyl)-4,11-dihydrobenzo[*g*]furo[3,4-*b*]quinoline-1,5,10(3*H*)-trione (5l).** Orange solid; yield: 343 mg (85%); mp 288–289 °C with decomp. IR (KBr)  $\nu_{\text{max}}/\text{cm}^{-1}$  3196, 3077, 2984, 2937, 2833, 1722, 1660, 1593, 1509, 1397, 1338, 1299, 1268, 1244, 1194, 1143, 1069, 1027, 1015, 939, 725, 672. <sup>1</sup>H NMR (DMSO-*d*<sub>6</sub>, 600 MHz):  $\delta = 10.57$  (s, 1H, NH), 8.04 (dd, 1H,  $J = 1.8, 7.2$  Hz), 7.88 (dd, 1H,  $J = 1.2, 7.2$  Hz), 7.84–7.77 (m, 2H), 6.90 (d, 1H,  $J = 1.8$  Hz), 6.80 (d, 1H,  $J = 8.4$  Hz), 6.75 (dd, 1H,  $J = 1.8, 8.4$  Hz), 4.98 (d, 1H,  $J = 16.8$  Hz), 4.92 (s, 1H), 4.87 (dd, 1H,  $J = 0.6, 16.8$  Hz), 3.71 (s, 3H, OCH<sub>3</sub>), 3.67 (s, 3H, OCH<sub>3</sub>). <sup>13</sup>C NMR (DMSO-*d*<sub>6</sub>, 150 MHz):  $\delta = 182.14, 179.56, 171.18, 155.62, 148.40, 147.66, 139.06, 137.18, 134.85, 133.30, 131.87, 130.19, 125.92, 125.72, 120.13, 118.42, 112.14, 111.76, 102.06, 65.99, 55.50, 55.47, 34.37$ . HRMS  $m/z$  [ $M - \text{H}$ ]<sup>−</sup> calcd for C<sub>23</sub>H<sub>16</sub>NO<sub>6</sub><sup>−</sup>: 402.0983; found: 402.0706.

**11-(3,4,5-Trimethoxyphenyl)-4,11-dihydrobenzo[*g*]furo[3,4-*b*]quinoline-1,5,10(3*H*)-trione (5m).** Red orange solid; yield: 372 mg (86%); mp 310–311 °C with decomp. IR (KBr)  $\nu_{\text{max}}/\text{cm}^{-1}$  3230, 3065, 3019, 2949, 2845, 1736, 1666, 1639, 1593, 1495, 1469, 1425, 1396, 1343, 1329, 1300, 1237, 1195, 1158, 1123, 1066, 1032, 1008, 933, 788, 737, 686. <sup>1</sup>H NMR (DMSO-*d*<sub>6</sub>, 600 MHz):  $\delta = 10.59$  (s, 1H, NH), 8.06 (dd, 1H,  $J = 1.2, 7.2$  Hz), 7.92 (dd, 1H,  $J = 1.2, 7.2$  Hz), 7.84–7.77 (dd, 1H,  $J = 1.8, 7.2$  Hz), 7.81 (dd, 1H,  $J = 1.2, 7.2$  Hz), 6.56 (s, 2H), 4.99 (d, 1H,  $J = 16.8$  Hz), 4.95 (s, 1H), 4.89 (dd, 1H,  $J = 0.6, 16.8$  Hz), 3.70 (s, 6H, 2 OCH<sub>3</sub>), 3.59 (s, 3H, OCH<sub>3</sub>). <sup>13</sup>C NMR (DMSO-*d*<sub>6</sub>, 150 MHz):  $\delta = 182.26, 179.59, 171.26, 155.92, 152.70$  (2C), 140.12, 139.47, 136.44, 134.90, 133.38, 131.91, 130.36, 126.01, 125.83, 118.01, 105.63 (2C), 101.87, 66.05, 59.88, 55.93 (2C), 35.23.

**11-(Pyridin-3-yl)-4,11-dihydrobenzo[*g*]furo[3,4-*b*]quinoline-1,5,10(3*H*)-trione (5n).** Red orange solid; yield: 279 mg (81%); mp 210–212 °C with decomp. IR (KBr)  $\nu_{\text{max}}/\text{cm}^{-1}$  3438, 2926, 1749, 1666, 1639, 1592, 1502, 1433, 1395, 1335, 1300, 1191, 1132, 1024, 1003, 928, 846, 788, 729, 640. <sup>1</sup>H NMR (DMSO-*d*<sub>6</sub>, 600 MHz):  $\delta = 10.70$  (s, 1H, NH), 8.06 (d, 1H,  $J = 2.4$  Hz), 8.37 (dd, 1H,  $J = 1.2, 4.8$  Hz), 8.08–8.05 (m, 1H), 7.81 (dd, 1H,  $J = 1.8, 7.8$  Hz), 7.82 (double-quint, 2H,  $J = 1.8, 7.8$  Hz), 7.75 (dt, 1H,  $J = 1.8, 7.8$  Hz), 7.30 (ddd, 1H,  $J = 0.6, 4.8, 7.8$  Hz), 5.07 (s, 1H), 5.99 (d, 1H,  $J = 16.8$  Hz), 4.91 (dd, 1H,  $J = 1.2, 16.8$  Hz). <sup>13</sup>C NMR (DMSO-*d*<sub>6</sub>, 150 MHz):  $\delta = 182.02, 179.35, 171.03, 156.35, 149.04, 147.55, 139.95, 139.72, 135.83, 134.86, 133.40, 131.80, 130.32, 125.99, 125.72, 123.59, 117.28, 101.17, 66.20, 33.10$ . HRMS  $m/z$  [ $M + \text{H}$ ]<sup>+</sup> calcd for C<sub>20</sub>H<sub>13</sub>N<sub>2</sub>O<sub>4</sub><sup>+</sup>: 345.0870; found: 345.0832 (−10.6 ppm).

**11-(5-Bromopyridin-2-yl)-4,11-dihydrobenzo[*g*]furo[3,4-*b*]quinoline-1,5,10(3*H*)-trione (5o).** Orange red solid; yield: 351 mg (83%); mp 274–275 °C with decomp. IR (KBr)  $\nu_{\text{max}}/\text{cm}^{-1}$



3065, 2925, 2856, 1740, 1669, 1636, 1601, 1497, 1473, 1395, 1333, 1299, 1190, 1160, 1131, 1095, 1008, 933, 858, 801, 756, 725, 669, 620.  $^1\text{H}$  NMR ( $\text{DMSO}-d_6$ , 600 MHz):  $\delta$  = 10.66 (s, 1H, NH), 8.52 (dd, 1H,  $J$  = 0.6, 2.4 Hz), 8.07 (dd, 1H,  $J$  = 1.2, 6.6 Hz), 7.99 (dd, 1H,  $J$  = 2.4, 8.4 Hz), 7.87 (td, 1H,  $J$  = 1.2, 7.2 Hz), 7.84 (dd, 1H,  $J$  = 1.2, 7.2 Hz), 7.82 (td, 1H,  $J$  = 1.8, 7.2 Hz), 7.53 (d, 1H,  $J$  = 7.8 Hz), 5.21 (s, 1H), 4.95 (d, 1H,  $J$  = 16.8 Hz), 4.91 (dd, 1H,  $J$  = 1.2, 16.8 Hz).  $^{13}\text{C}$  NMR ( $\text{DMSO}-d_6$ , 125 MHz):  $\delta$  = 182.16, 179.59, 171.18, 160.50, 156.60, 149.90, 139.83, 138.91, 135.17, 133.60, 131.73, 130.07, 126.15, 125.85, 124.88, 118.47, 118.16, 100.66, 66.27, 37.36. HRMS  $m/z$   $[\text{M} + \text{H}]^+$  calcd for  $\text{C}_{20}\text{H}_{12}\text{BrN}_2\text{O}_4^+$ : 422.9975 and 424.9955; found: 422.9925 and 424.9915 (−11.8 ppm).

### Cell line and culture conditions

The human lung LU-1 cancer (ATCC HTB-57 TM), lung A549 cancer, epidermoid carcinoma (KB, ATCC number CCL-17), hepatocellular carcinoma (HepG2, ATCC number HB-8065), breast (MCF7, HTB-22<sup>TM</sup>) cancer cell lines, and human embryonic kidney (HEK-293, ATCC number CRL-1573) cell line were purchased from the American Type Culture Collection (ATCC, Manassas, VA, USA). These cell lines were stored in liquid nitrogen, cultured in DMEM (Dulbeccos Modified Eagle Medium) medium with 7–10% fetal bovine serum (Gibco, USA), and 100 U per mL penicillin, and 100  $\mu\text{g mL}^{-1}$  streptomycin (Gibco, USA) in a humidified atmosphere with 5%  $\text{CO}_2$  at 37 °C. The cells in the log phase are preferentially used for the tests.

### MTT assay

MTT (3-(4,5-dimethylthiazol-2-yl)-2,5-diphenyltetrazolium bromide) assay was used to evaluate cytotoxicity of compounds **5** against epidermoid carcinoma (KB, ATCC number CCL-17), hepatocellular carcinoma (HepG2, ATCC number HB-8065), lung (A549) cancer, breast (MCF7, HTB-22<sup>TM</sup>) cancer cell lines, and human embryonic kidney (HEK-293, ATCC number CRL-1573) cell line. Human cancer cell lines were seeded at  $3 \times 10^4$  cells per mL, incubated for 3 days in the presence of the series of concentration 1.00, 0.25, 0.0625, and 0.0156  $\mu\text{g mL}^{-1}$  of derivatives **5** in DMSO. 10  $\mu\text{L}$  solution of 5 mg  $\text{mL}^{-1}$  MTT in sodium phosphate buffer (PBS, 0.1 M, pH 7.4) was then added to each well of the reaction plate, incubated at 37 °C for 4 h, and carefully aspirated. 150  $\mu\text{L}$  of DMSO was added to each well to dissolve the obtained formazan crystals. A Biotek Epoch 2 microplate reader was used to determine the absorbance of the solutions at 540 nm wavelength. The percentage of cell growth inhibition of compounds **5** was measured by the decrease in absorbance compared to the absorbance observed for the control samples without compounds tested.

### Cell cycle analysis

Lung SK-LU-1 cancer cells seeded in 25  $\text{cm}^2$  flasks (Corning, USA) at a density of  $3 \times 10^5$  cells, were incubated with tested samples at 0.08  $\mu\text{M}$ , 0.16  $\mu\text{M}$  and 0.32  $\mu\text{M}$ , DMSO 0.05% (negative reference) and Ellipticine 1.3  $\mu\text{M}$ , Vincristine 0.4  $\mu\text{M}$  and 4  $\mu\text{M}$  (positive control) for 24 h. The cells were then harvested, suspended 2 times with phosphate-buffered saline

(PBS), fixed with ice-cold ethanol 70% at −20 °C in 2 h, low-speed centrifuged at 2000 rpm in 5 min to collect. The treated cells were washed and then diluted with 0.45 mL PBS, incubated with RNase A (1 mg  $\text{mL}^{-1}$ ) at 37 °C in 15 min, stained with 25  $\mu\text{L}$  propidium iodide (PI) (1 mg  $\text{mL}^{-1}$ ) in 30 minute and diluted with 500  $\mu\text{L}$  PBS. Flow cytometry Novocyte (ACEA Biosciences, San Diego, CA, USA) with data analyzed & reported by ACEA's NovoExpress software was used to analyze samples for apoptosis.

### Cell nucleus staining with Hoechst 33342 for apoptosis

190 mL of suspension human lung SK-LU-1 cancer cells were grown in a 96-well plate at 37 °C in 24 h and then incubated with compounds **5a**, **5b** at different concentrations. Ellipticine 1.3 ( $\mu\text{M}$ ) and Vincristine (0.4  $\mu\text{M}$  and 4.0  $\mu\text{M}$ ) were used as a reference; DMSO 0.5% was used as a negative control. After 24 h of incubation, the cells were fixed with formaldehyde 4%. After 30 min, the cells were washed again with PBS and stained with Hoechst 33342 (0.5  $\mu\text{g mL}^{-1}$ ) for 10 min. Cells were observed by fluorescence microscopy at an excitation wavelength of 350 nm and an emission wavelength of 461 nm. Apoptosis cells are defined as cells with brighter nuclei (due to condensed chromatin) or nuclei that are fragmented.

### Caspase-3/7 assays

ApoONE® Homogeneous Caspase-3/7 Kit (Promega, USA) was used to assess the effect of compounds **5a**, **5b** on caspase-3/7 activation in human lung SK-LU-1 cancer cells. 50  $\mu\text{L}$  of SK-LU-1 cells were plated on a 96-well plate with cell concentration of  $2 \times 10^5$  cells per well, followed by adding 50  $\mu\text{L}$  of compounds **5a**, **5b** at various concentrations to the wells. Ellipticine (1.3  $\mu\text{M}$ ), and Vincristine (4  $\mu\text{M}$ ) were used as a positive control and dissolved solvent for blank. The mixture was incubated in a humidified atmosphere of 5%  $\text{CO}_2$  at 37 °C for 5 h. Next, 100  $\mu\text{L}$  of Apo-ONE® Caspase-3/7 reagent was pipetted into each well, a plate shaker was used to mix gently the contents of the wells at 350 rpm for 30 seconds, and then the plate was kept at room temperature for 1–18 h. Using a Tecan GENios Pro microplate reader to measure the relative fluorescence units (RFU) at the wavelength range of excitation ( $485 \pm 20$  nm) and emission ( $530 \pm 25$  nm). The activation of caspase-3/7, directly proportional to fluorescence, was calculated by the following formula: caspase activity = RFU value of tested sample – RFU value of the blank.

### Annexin V FITC and PI flow cytometry assay for apoptosis

The Kit Annexin V and PI/dead cell apoptosis® from Invitrogen was used to assess the effect of compounds **5a**, **5b** on the percentage of the apoptotic cells in SK-LU-1 human cancer cells. Briefly, Lung SK-LU-1 cancer cells seeded in 25  $\text{cm}^2$  flasks (Corning, USA) at a density of  $3 \times 10^5$  cells were incubated with test samples at different concentrations, DMSO 0.5%, Ellipticine 1.3  $\mu\text{M}$ , Vincristine 0.4  $\mu\text{M}$  and 4  $\mu\text{M}$  in 24 h then collected into falcon tubes. After centrifugation, the cell was washed with cold PBS. The washed cell was re-centrifuged, discarded the supernatant, re-suspended in 100  $\mu\text{L}$  of 1X annexin-binding





buffer, and then added 5  $\mu\text{L}$  of FITC annexin V and 1  $\mu\text{L}$  of the 100  $\mu\text{g mL}^{-1}$  PI working solution. Incubation of the cells was performed for 15 min at room temperature; followed by adding 400  $\mu\text{L}$  of 1X annexin-binding buffer. The stained cells were then analyzed by a Novocyte flow cytometry system.

### Molecular docking study

Two docking assays were performed in order to investigate the anti-tubulin and caspase activating mechanism of synthesized compounds. To do so, crystal structures of tubulin-colchicine complex (PDB ID: 4O2B)<sup>80</sup> and procaspase-6 (PDB ID: 4FXO)<sup>69</sup> have been retrieved from the Protein Data Bank (<https://www.rcsb.org/>). Ligand structures were built in 3D conformations using MOE 2015.10.<sup>81</sup> All the docking procedures were carried out following the same protocol previously reported.<sup>71,82</sup> For the tubulin docking simulations,  $\alpha 1/\beta 1$  heterodimers were retained and protonated using MOE. The binding pocket was centered on the colchicine binding site located at the  $\beta$ -tubulin dimer. The interface residues were determined following three-zone hypothesis of Massaroti *et al.*<sup>65</sup> Colchicine was used as reference compound for these docking assays. According to the procaspase/caspase activation, active ligands must show chelating ability against inhibitory Zn ion in the catalytic domain site. The interaction of newly synthesized compounds was compared with the procaspase activating compound 1 (PAC-1).<sup>83</sup> Importantly, docking simulations were performed keeping all the water molecules that interact with Zn as they also play a role in the complex with the ligands.<sup>69</sup> For the estimation of negative binding energy (kcal  $\text{mol}^{-1}$ ), a MOE's built-in GBVI/WSA scoring function was applied and the computed values were compared with those obtained for the reference compounds.<sup>81</sup> The geometries of docking poses could be visualized using BIOVIA Discovery Studio Visualizer (DSV) 2020.<sup>84</sup>

### Physicochemical and ADMET prediction

Herein, important physicochemical properties and those associated to the Absorption, Distribution, Metabolism, Excretion and Toxicity (ADMET) processes were estimated by using potential cheminformatics tools, including ADMETlab 2.0 and 3PRule.<sup>75,76</sup> In particular, oral absorption profiles were characterized using the Provisional Biopharmaceutical Classification System (PBCS).<sup>77</sup> Furthermore, several global ADMET score compliance such as Lipinski Rule of Five (Ro5),<sup>85</sup> bioavailability score,<sup>78</sup> and other toxicological rules were analyzed in consensus for examining their drug-likeness profiles.<sup>79</sup>

## Conclusions

The efficient synthesis of podophyllotoxin-naphthoquinone derivatives using microwave-promoted three-component reactions from 2-amino-1,4-naphthoquinone, tetronic acid, and (hetero)aromatic aldehydes in glacial acetic acid and 20 mol% of *p*-TsOH has been described. Most of synthesized podophyllotoxin-naphthoquinone compounds **5a–o** exhibited inhibitory effect on human cancer cell lines employed in this

study. The most potent cytotoxic podophyllotoxin-naphthoquinone compounds **5a** and **5b** were found to possess anti-proliferative activity through concentration-dependently inducing cell cycle arrest at G2/M phase, caspase-3/7 activation, and apoptosis as well. Moreover, molecular docking studies exhibited importance interaction of two compounds against residues in the colchicine-binding-site of tubulin. These preliminary results revealed that podophyllotoxin-naphthoquinone compounds are worthy of further study aiming to develop new potential anticancer agents.

## Author contributions

Ha Thanh Nguyen: project administration: conceptual design; writing – original draft. Quynh Giang Nguyen Thi and Phuong Hoang Thi: investigation: synthesis and characterizations of compounds. Thu Ha Nguyen Thi and Tuyet Anh Dang Thi: investigation: biological activity evaluation of potent compounds. Giang Le-Nhat-Thuy: investigation: revised draft. Bao Le-Quang and Hai Pham-The: investigation: molecular docking studies. Tuyen Van Nguyen: supervision: conceptual design; writing – review & editing.

## Conflicts of interest

There are no conflicts to declare.

## Acknowledgements

This work was supported by Vietnam Academy of Science and Technology [Grant number CT0000.03/22-23].

## Notes and references

- 1 R. A. Stanton, K. M. Gernert, J. H. Nettles and R. Aneja, Drugs that target dynamic microtubules: a new molecular perspective: targeting microtubule dynamics, *Med. Res. Rev.*, 2011, **31**, 443–481.
- 2 F. Pellegrini and D. R. Budman, Review: Tubulin Function, Action of Antitubulin Drugs, and New Drug Development, *Cancer Invest.*, 2005, **23**, 264–273.
- 3 T. Imbert, Discovery of podophyllotoxins, *Biochimie*, 1998, **80**, 207–222.
- 4 J. D. L. oik and S. B. Horwitz, Effects of podophyllotoxin and VP-16-213 on microtubule assembly *in vitro* and nucleoside transport in HeLa cells, *Biochemistry*, 1976, **15**, 5435–5443.
- 5 M. Gordaliza, M. A. Castro, J. M. Miguel del Corral and A. San Feliciano, Antitumor properties of podophyllotoxin and related compounds, *Curr. Pharm. Des.*, 2000, **6**, 1811–1839.
- 6 Y. Qian Liu, L. Yang and X. Tian, Podophyllotoxin: current perspectives, *Curr. Bioact. Compd.*, 2007, **3**, 37–66.
- 7 M. Gordaliza, P. A. García, J. M. Miguel del Corral, M. A. Castro and M. A. Gómez-Zurita, Podophyllotoxin: distribution, sources, applications and new cytotoxic derivatives, *Toxicon*, 2004, **44**, 441–459.





- 8 Y. You, Podophyllotoxin Derivatives: Current Synthetic Approaches for New Anticancer Agents, *Curr. Pharm. Des.*, 2005, **11**, 1695–1717.
- 9 N. Jeedimalla, M. Flint, L. Smith, A. Haces, D. Minond and S. P. Roche, Multicomponent assembly of 4-azapodophyllotoxins: a fast entry to highly selective and potent anti-leukemic agents, *Eur. J. Med. Chem.*, 2015, **106**, 167–179.
- 10 I. V. Magedov, M. Manpadi, S. Van slambrouck, W. F. A. Steelant, E. Rozhkova, N. M. Przheval'skii, S. Rogelj and A. Kornienko, Discovery and investigation of antiproliferative and apoptosis-inducing properties of new heterocyclic podophyllotoxin analogues accessible by a one-step multicomponent synthesis, *J. Med. Chem.*, 2007, **50**, 5183–5192.
- 11 Y. Hitotsuyanagi, M. Fukuyo, K. Tsuda, M. Kobayashi, A. Ozeki, H. Itokawa and K. Takeya, 4-Aza-2,3-dehydro-4-deoxypodophyllotoxins: simple aza-podophyllotoxin analogues possessing potent cytotoxicity, *Bioorg. Med. Chem. Lett.*, 2000, **10**, 315–317.
- 12 H. T. Nguyen, G. Le-Nhat-Thuy, P. Hoang Thi, Q. G. Nguyen Thi, T. A. Nguyen, T. H. Nguyen Thi, T. A. Dang Thi and T. V. Nguyen, Microwave-Assisted Three-Component Synthesis of Novel *N*-Arylated-Dihydrobenzo[*g*]quinoline-5,10-Diones and Their Potential Cytotoxic Activity, *Chem. Biodivers.*, 2022, DOI: [10.1002/cbdv.202200359](https://doi.org/10.1002/cbdv.202200359).
- 13 N. B. Chernysheva, D. V. Tsyganov, A. A. Philchenkov, M. P. Zavelevich, A. S. Kiselyov, R. V. Semenov, M. N. Semenova and V. V. Semenov, Synthesis and comparative evaluation of 4-oxa- and 4-azapodophyllotoxins as antiproliferative microtubule destabilizing agents, *Bioorg. Med. Chem. Lett.*, 2012, **22**, 2590–2593.
- 14 M. G. Botes, S. C. Pelly, M. A. L. Blackie, A. Kornienko and W. A. L. van Otterlo, Synthesis of 4-azapodophyllotoxins with anticancer activity by multicomponent reactions (Review), *Chem. Heterocycl. Compd.*, 2014, **50**, 119–138.
- 15 A. Kamal, P. Suresh, A. Mallareddy, B. A. Kumar, P. V. Reddy, P. Raju, J. R. Tamboli, T. B. Shaik, N. Jain and S. V. Kalivendi, Synthesis of a new 4-aza-2,3-didehydropodophyllotoxin analogues as potent cytotoxic and antimetabolic agents, *Bioorg. Med. Chem.*, 2011, **19**, 2349–2358.
- 16 M. N. Semenova, A. S. Kiselyov, D. V. Tsyganov, L. D. Konyushkin, S. I. Firgang, R. V. Semenov, O. R. Malyshev, M. M. Raihstat, F. Fuchs, A. Stielow, M. Lantow, A. A. Philchenkov, M. P. Zavelevich, N. S. Zefirov, S. A. Kuznetsov and V. V. Semenov, Polyalkoxybenzenes from plants. 5. Parsley seed extract in synthesis of azapodophyllotoxins featuring strong tubulin destabilizing activity in the sea urchin embryo and cell culture assays, *J. Med. Chem.*, 2011, **54**, 7138–7149.
- 17 A. Kamal, J. R. Tamboli, V. L. Nayak, S. F. Adil, M. V. P. S. Vishnuvardhan and S. Ramakrishna, Synthesis of a terphenyl substituted 4-aza-2,3-didehydropodophyllotoxin analogues as inhibitors of tubulin polymerization and apoptosis inducers, *Bioorg. Med. Chem.*, 2014, **22**, 2714–2723.
- 18 R. Labruère, B. Gautier, M. Testud, J. Seguin, C. Lenoir, S. Desbène-Finck, P. Helissey, C. Garbay, G. G. Chabot, M. Vidal and S. Giorgi-Renault, Design, synthesis, and biological evaluation of the first podophyllotoxin analogues as potential vascular-disrupting agents, *ChemMedChem*, 2010, **5**, 2016–2025.
- 19 A. Kumar, V. Kumar, A. E. Alegria and S. V. Malhotra, N-Hydroxyethyl-4-aza-didehydropodophyllotoxin derivatives as potential antitumor agents, *Eur. J. Pharm. Sci.*, 2011, **44**, 21–26.
- 20 J. Frackenpohl, I. Adelt, H. Antonicek, C. Arnold, P. Behrmann, N. Blaha, J. Böhmer, O. Gutbrod, R. Hanke, S. Hohmann, M. van Houtdrevre, P. Lösel, O. Malsam, M. Melchers, V. Neufert, E. Peschel, U. Reckmann, T. Schenke, H.-P. Thiesen, R. Velten, K. Vogelsang and H.-C. Weiss, Insecticidal heterolignans—Tubuline polymerization inhibitors with activity against chewing pests, *Bioorg. Med. Chem.*, 2009, **17**, 4160–4184.
- 21 S. Gupta, L. Das, A. B. Datta, A. Poddar, M. E. Janik and B. Bhattacharyya, Oxalone and lactone moieties of podophyllotoxin exhibit properties of both the B and C rings of colchicine in its binding with tubulin, *Biochemistry*, 2006, **45**, 6467–6475.
- 22 D. Imperio, T. Pirali, U. Galli, F. Pagliai, L. Cafici, P. L. Canonico, G. Sorba, A. A. Genazzani and G. C. Tron, Replacement of the lactone moiety on podophyllotoxin and steganacin analogues with a 1,5-disubstituted 1,2,3-triazole via ruthenium-catalyzed click chemistry, *Bioorg. Med. Chem.*, 2007, **15**, 6748–6757.
- 23 X. Yang, C. Zhang and L. Wu, L-Proline catalyzed three-component synthesis of para-naphthoquinone-4-azapodophyllotoxin hybrids as potent antitumor agents, *RSC Adv.*, 2015, **5**, 18945–18951.
- 24 D. S. Donawade, A. V. Raghu and G. S. Gadaginamath, Synthesis and antimicrobial activity of some new 1-substituted-3-pyrrolyl aminocarbonyl/oxadiazolyl/triazolyl/5-methoxy-2-methylindoles and benz[*g*]indoles, *Indian J. Chem., Sect. B*, 2006, **45**, 689–696.
- 25 D. S. Donawade, A. V. Raghu and G. S. Gadaginamath, Synthesis and antimicrobial activity of novel linearly fused 5-substituted-7-acetyl-2,6-dimethyloxazolo[4,5-*f*]indoles, *Indian J. Chem., Sect. B*, 2007, **46**, 690–693.
- 26 D. S. Donawade, A. V. Raghu, U. M. Muddapur and G. S. Gadaginamath, Chemoselective reaction of benz(*g*) indole based bisheterocycle dicarboxylate towards hydrazine hydrate: synthesis and antimicrobial activity of new triheterocycles-5-pyrrolylaminocarbonyl/mercaptooxadiazolyl/4-allyl-5-me rcaptotriazolylmethoxy-1-furfuryl-2-methylbenz(*g*)indoles, *Indian J. Chem., Sect. B*, 2005, **44**, 1470–1475.
- 27 T. A. Dang Thi, N. T. Kim Tuyet, C. Pham The, H. Thanh Nguyen, C. Ba Thi, H. Thi Phuong, L. Van Boi, T. Van Nguyen and M. D'hooghe, Synthesis and cytotoxic evaluation of novel amide-triazole-linked triterpenoid-AZT conjugates, *Tetrahedron Lett.*, 2015, **56**, 218–224.
- 28 G. Le-Nhat-Thuy, T. A. Dang Thi, Q. G. Nguyen Thi, P. Hoang Thi, T. A. Nguyen, H. T. Nguyen, T. H. Nguyen Thi,



- H. S. Nguyen and T. V. Nguyen, Synthesis and biological evaluation of novel benzo[a]pyridazino[3,4-c]phenazine derivatives, *Bioorg. Med. Chem. Lett.*, 2021, **43**, 128054.
- 29 T. A. Dang Thi, L. Decuyper, H. Thi Phuong, D. Vu Ngoc, H. Thanh Nguyen, T. Thanh Nguyen, T. Do Huy, H. Huy Nguyen, M. D'hooghe and T. Van Nguyen, Synthesis and cytotoxic evaluation of novel dihydrobenzo[h]cinnoline-5,6-diones, *Tetrahedron Lett.*, 2015, **56**, 5855–5858.
  - 30 Z. Liu, Z. Zhang, W. Zhang and D. Yan, 2-Substituted-1-(2-morpholinoethyl)-1H-naphtho[2,3-d]imidazole-4,9-diones: design, synthesis and antiproliferative activity, *Bioorg. Med. Chem. Lett.*, 2018, **28**, 2454–2458.
  - 31 J. Zhang, S. Wang, Y. Ba and Z. Xu, 1,2,4-Triazole-quinoline/quinolone hybrids as potential anti-bacterial agents, *Eur. J. Med. Chem.*, 2019, **174**, 1–8.
  - 32 N. Kerru, L. Gummidi, S. Maddila, K. K. Gangu and S. B. Jonnalagadda, A review on recent advances in nitrogen-containing molecules and their biological applications, *Molecules*, 2020, **25**, 1909.
  - 33 G. Burckhardt, A. Walter, H. Triebel, K. Störl, H. Simon, J. Störl, A. Opitz, E. Roemer and C. Zimmer, Binding of 2-azaanthraquinone derivatives to DNA and their interference with the activity of DNA topoisomerases *in vitro*, *Biochemistry*, 1998, **37**, 4703–4711.
  - 34 V. Marković, N. Debeljak, T. Stanojković, B. Kolundžija, D. Sladić, M. Vujčić, B. Janović, N. Tanić, M. Perović, V. Tešić, J. Antić and M. D. Joksović, Anthraquinone-chalcone hybrids: synthesis, preliminary antiproliferative evaluation and DNA-interaction studies, *Eur. J. Med. Chem.*, 2015, **89**, 401–410.
  - 35 N. Khan, F. Afroz, M. N. Begum, S. Roy Rony, S. Sharmin, F. Moni, C. Mahmood Hasan, K. Shaha and Md. H. Sohrab, Endophytic *Fusarium solani*: A rich source of cytotoxic and antimicrobial naphthaquinone and azaanthraquinone derivatives, *Toxicol. Rep.*, 2018, **5**, 970–976.
  - 36 D. Cappoen, E. Torfs, T. Meiresonne, P. Claes, E. Semina, F. Holvoet, M. B. de Macedo, F. Cools, T. Pillier, A. Matheeußen, K. Van Calster, G. Caljon, P. Delpitte, L. Maes, O. Neyrolles, N. De Kimpe, S. Mangelinckx and P. Cos, The synthesis and *in vitro* biological evaluation of novel fluorinated tetrahydrobenzo[j]phenanthridine-7,12-diones against *Mycobacterium tuberculosis*, *Eur. J. Med. Chem.*, 2019, **181**, 111549.
  - 37 J. Wang, W. Li, J. Qin, L. Wang, S. Wei and H. Tang, Assessment of novel azaanthraquinone derivatives as potent multi-target inhibitors of inflammation and amyloid- $\beta$  aggregation in Alzheimer's disease, *Bioorg. Chem.*, 2019, **83**, 477–486.
  - 38 P. Thanuphol, Y. Asami, K. Shiomi, A. Wongnoppavich, P. Tuchinda, N. Soonthornchareonnon and G. Marcanine, A new cytotoxic 1-azaanthraquinone from the stem bark of *Goniothalamus marcanii* Craib, *Nat. Prod. Res.*, 2018, **32**, 1682–1689.
  - 39 G. Powis, Metabolism and reactions of quinoid anticancer agents, *Pharmacol. Ther.*, 1987, **35**, 57–162.
  - 40 J. L. Bolton and T. Dunlap, Formation and biological targets of quinones: cytotoxic versus cytoprotective effects, *Chem. Res. Toxicol.*, 2017, **30**, 13–37.
  - 41 D. Barasch, O. Zipori, I. Ringel, I. Ginsburg, A. Samuni and J. Katzhendler, Novel anthraquinone derivatives with redox-active functional groups capable of producing free radicals by metabolism: are free radicals essential for cytotoxicity?, *Eur. J. Med. Chem.*, 1999, **34**, 597–615.
  - 42 L. G. Fedenok, K. Yu. Fedotov, E. A. Pritchina and N. E. Polyakov, In situ generated reagent from sulfur for alkynylantraquinone cyclization. The simple synthesis of angular thienoanthraquinones, *Tetrahedron Lett.*, 2016, **57**, 1273–1276.
  - 43 W.-X. Sun, Y.-J. Ji, Y. Wan, H.-W. Han, H.-Y. Lin, G.-H. Lu, J.-L. Qi, X.-M. Wang and Y.-H. Yang, Design and synthesis of piperazine acetate podophyllotoxin ester derivatives targeting tubulin depolymerization as new anticancer agents, *Bioorg. Med. Chem. Lett.*, 2017, **27**, 4066–4074.
  - 44 H.-W. Han, H.-Y. Qiu, C. Hu, W.-X. Sun, R.-W. Yang, J.-L. Qi, X.-M. Wang, G.-H. Lu and Y.-H. Yang, Design, synthesis and anti-cancer activity evaluation of podophyllotoxin-norcantharidin hybrid drugs, *Bioorg. Med. Chem. Lett.*, 2016, **26**, 3237–3242.
  - 45 A. Kamal, J. R. Tamboli, M. J. Ramaiah, S. F. Adil, S. N. C. V. L. Pushpavalli, R. Ganesh, P. Sarma, U. Bhadra and M. Pal-Bhadra, Quinazolino linked 4 $\beta$ -amidopodophyllotoxin conjugates regulate angiogenic pathway and control breast cancer cell proliferation, *Bioorg. Med. Chem. Lett.*, 2013, **21**, 6414–6426.
  - 46 Q. G. Nguyen Thi, G. Le-Nhat-Thuy, T. A. Dang Thi, P. Hoang Thi, A. Nguyen Tuan, T. H. Nguyen Thi, T. T. Nguyen, T. Nguyen Ha, H. Hoang Mai and T. V. Nguyen, Synthesis of novel potent cytotoxicity podophyllotoxin-naphthoquinone compounds via microwave-assisted multicomponent domino reactions, *Bioorg. Med. Chem. Lett.*, 2021, **37**, 127841.
  - 47 T. Otto and P. Sicinski, Cell cycle proteins as promising targets in cancer therapy, *Nat. Rev. Cancer*, 2017, **17**, 93–115.
  - 48 J. R. Jackson, D. R. Patrick, M. M. Dar and P. S. Huang, Targeted anti-mitotic therapies: can we improve on tubulin agents?, *Nat. Rev. Cancer*, 2007, **7**, 107–117.
  - 49 P.-L. Kuo, Y.-L. Hsu, C.-H. Chang and C.-C. Lin, The mechanism of ellipticine-induced apoptosis and cell cycle arrest in human breast MCF-7 cancer cells, *Cancer Lett.*, 2005, **223**, 293–301.
  - 50 J. B. Le Pecq, Nguyen-Dat-Xuong, C. Gosse and C. Paoletti, A new antitumoral agent: 9-hydroxyellipticine. Possibility of a rational design of anticancerous drugs in the series of DNA intercalating drugs, *Proc. Natl. Acad. Sci. U. S. A.*, 1974, **71**, 5078–5082.
  - 51 V. M. Dan, T. S. Varghese, G. Viswanathan and S. Baby, Ellipticine, its derivatives: re-evaluation of clinical suitability with the aid of drug delivery systems, *Curr. Cancer Drug Targets*, 2020, **20**, 33–46.
  - 52 X.-S. Huo, X.-E. Jian, J. Ou-Yang, L. Chen, F. Yang, D.-X. Lv, W.-W. You, J.-J. Rao and P.-L. Zhao, Discovery of highly potent tubulin polymerization inhibitors: design,



- synthesis, and structure-activity relationships of novel 2,7-diaryl-[1,2,4]triazolo[1,5-a]pyrimidines, *Eur. J. Med. Chem.*, 2021, **220**, 113449.
- 53 S. W. Lowe and A. W. Lin, Apoptosis in cancer, *Carcinogenesis*, 2000, **21**, 485–495.
  - 54 S. Allen, J. Sotos, M. J. Sylte and C. J. Czuprynski, Use of Hoechst 33342 staining to detect apoptotic changes in bovine mononuclear phagocytes infected with *Mycobacterium avium* subsp. *Paratuberculosis*, *Clin. Diagn. Lab. Immunol.*, 2001, **8**, 460–464.
  - 55 Y. Errami, A. S. Naura, H. Kim, J. Ju, Y. Suzuki, A. H. El-Bahrawy, M. A. Ghonim, R. A. Hemeida, M. S. Mansy, J. Zhang, M. Xu, M. E. Smulson, H. Brim and A. H. Boulares, Apoptotic DNA fragmentation may be a cooperative activity between caspase-activated deoxyribonuclease and the poly(ADP-ribose) polymerase-regulated DNAS1L3, an endoplasmic reticulum-localized endonuclease that translocates to the nucleus during apoptosis, *J. Biol. Chem.*, 2013, **288**, 3460–3468.
  - 56 S. Elmore, Apoptosis: a review of programmed cell death, *Toxicol Pathol.*, 2007, **35**, 495–516.
  - 57 A. G. Porter and R. U. Jänicke, Emerging roles of caspase-3 in apoptosis, *Cell Death Differ.*, 1999, **6**, 99–104.
  - 58 S. Shalini, L. Dorstyn, S. Dawar and S. Kumar, Old, new and emerging functions of caspases, *Cell Death Differ.*, 2015, **22**, 526–539.
  - 59 V. A. Fadok, D. L. Bratton, S. C. Frasch, M. L. Warner and P. M. Henson, The role of phosphatidylserine in recognition of apoptotic cells by phagocytes, *Cell Death Differ.*, 1998, **5**, 551–562.
  - 60 H. A. Andree, C. P. Reutelingsperger, R. Hauptmann, H. C. Hemker, W. T. Hermens and G. M. Willems, Binding of vascular anticoagulant alpha (VAC alpha) to planar phospholipid bilayers, *J. Biol. Chem.*, 1990, **265**, 4923–4928.
  - 61 N. H. Thanh, N. T. Thu Ha, N. T. Tra, L. T. Tu Anh, N. The Son, N. V. Tuyen and P. Van Kiem, Bannaxanthone E induced cell-cycle arrest and apoptosis in human lung cancer cell line, *Nat. Prod. Commun.*, 2021, **16**, 1934578X2110590.
  - 62 G. Majno and I. Joris, Apoptosis, Oncosis, and Necrosis. An overview of cell death, *Am. J. Pathol.*, 1995, **146**, 3–15.
  - 63 G. T. Vidyavathi, B. V. Kumar, A. V. Raghu, T. Aravinda, U. Hani, H. C. A. Murthy and A. H. Shridhar, Punica granatum pericarp extract catalyzed green chemistry approach for synthesizing novel ligand and its metal(II) complexes: molecular docking/DNA interactions, *J. Mol. Struct.*, 2022, **1249**, 131656.
  - 64 R. Raveesha, A. M. Anusuya, A. V. Raghu, K. Yogesh Kumar, M. G. Dileep Kumar, S. B. Benaka Prasad and M. K. Prashanth, Synthesis and characterization of novel thiazole derivatives as potential anticancer agents: Molecular docking and DFT studies, *Comput. Toxicol.*, 2022, **21**, 100202.
  - 65 A. Massarotti, A. Coluccia, R. Silvestri, G. Sorba and A. Brancale, The tubulin colchicine domain: a molecular modeling perspective, *ChemMedChem*, 2012, **7**, 33–42.
  - 66 W. Li, H. Sun, S. Xu, Z. Zhu and J. Xu, Tubulin inhibitors targeting the colchicine binding site: a perspective of privileged structures, *Future Med. Chem.*, 2017, **9**, 1765–1794.
  - 67 A. V. Raghu, G. S. Gadaginamath, N. T. Mathew, S. B. Halligudi and T. M. Aminabhavi, Synthesis and characterization of novel polyurethanes based on 4,4'-[1,4-phenylenedi-diazene-2,1-diyl]bis(2-carboxyphenol) and 4,4'-[1,4-phenylenedi-diazene-2,1-diyl]bis(2-chlorophenol) hard segments, *React. Funct. Polym.*, 2007, **67**, 503–514.
  - 68 A. V. Raghu, G. S. Gadaginamath, S. S. Jawalkar, S. B. Halligudi and T. M. Aminabhavi, Synthesis, characterization, and molecular modeling studies of novel polyurethanes based on 2,2'-[ethane-1,2-diylbis(nitrilomethylidene)]diphenol and 2,2'-[hexane-1,6-diylbis(nitrilomethylidene)] diphenol hard segments, *J. Polym. Sci. 1 Polym. Chem.*, 2006, **44**, 6032–6046.
  - 69 E. M. Velázquez-Delgado and J. A. Hardy, Zinc-mediated allosteric inhibition of caspase-6, *J. Biol. Chem.*, 2012, **287**, 36000–36011.
  - 70 H. Pham-The, M. Á. Cabrera-Pérez, N.-H. Nam, J. A. Castillo-Garit, B. Rasulev, H. Le-Thi-Thu and G. M. Casañola-Martin, In silico assessment of ADME properties: advances in Caco-2 cell monolayer permeability modelling, *Curr. Top. Med. Chem.*, 2019, **18**, 2209–2229.
  - 71 L. C. Huan, P.-T. Tran, C. V. Phuong, P. H. Duc, D. T. Anh, P. T. Hai, L. T. T. Huong, N. T. Thuan, H. J. Lee, E. J. Park, J. S. Kang, N. P. Linh, T. T. Hieu, D. T. K. Oanh, S.-B. Han and N.-H. Nam, Novel 3,4-dihydro-4-oxoquinazoline-based acetohydrazides: design, synthesis and evaluation of antitumor cytotoxicity and caspase activation activity, *Bioorg. Chem.*, 2019, **92**, 103202.
  - 72 L. C. Huan, C. V. Phuong, L. C. Truc, V. N. Thanh, H. Pham-The, L.-T.-T. Huong, N. T. Thuan, E. J. Park, A. Y. Ji, J. S. Kang, S.-B. Han, P.-T. Tran and N.-H. Nam, (E)-N'-Arylidene-2-(4-oxoquinazolin-4(3H)-yl) acetohydrazides: synthesis and evaluation of antitumor cytotoxicity and caspase activation activity, *J. Enzyme Inhib. Med. Chem.*, 2019, **34**, 465–478.
  - 73 S. B. Benaka Prasad, S. Naveen, C. S. Ananda Kumar, N. K. Lokanath, A. V. Raghu, I. Daraghmeah, K. R. Reddy and I. Warad, Synthesis, structural exploration, spectral and combinatorial analysis of racemic-3-isobutyl-5-phenyl-5-(pyridin-4-yl)imida-zolidine-2,4-dione: comparison between experimental and DFT calculations, *J. Mol. Struct.*, 2018, **1167**, 215–226.
  - 74 B. Pramodh, P. Naresh, S. Naveen, N. K. Lokanath, S. Ganguly, J. Panda, S. Murugesan, A. V. Raghu and I. Warad, Synthesis, spectral characterization, crystal structure and theoretical investigation of (E)-3-(4-bromothiophen-2-yl)-1-(5-bromothiophen-2-yl)prop-2-en-1-one, *Chem. Data Collect.*, 2021, **31**, 100587.
  - 75 G. Xiong, Z. Wu, J. Yi, L. Fu, Z. Yang, C. Hsieh, M. Yin, X. Zeng, C. Wu, A. Lu, X. Chen, T. Hou and D. Cao, ADMETlab 2.0: an integrated online platform for accurate and comprehensive predictions of ADMET properties, *Nucleic Acids Res.*, 2021, **49**, W5–W14.



- 76 H. Pham-The, I. González-Álvarez, M. Bermejo, T. Garrigues, H. Le-Thi-Thu and M. Á. Cabrera-Pérez, The use of rule-based and QSPR approaches in ADME profiling: a case study on Caco-2 permeability, *Mol. Inf.*, 2013, **32**, 459–479.
- 77 H. Pham-The, T. Garrigues, M. Bermejo, I. González-Álvarez, M. C. Monteagudo and M. Á. Cabrera-Pérez, Provisional classification and *in silico* study of biopharmaceutical system based on Caco-2 cell permeability and dose Number, *Mol. Pharm.*, 2013, **10**, 2445–2461.
- 78 Y. C. Martin, A Bioavailability Score, *J. Med. Chem.*, 2005, **48**, 3164–3170.
- 79 M. C. Sanguinetti and M. Tristani-Firouzi, hERG potassium channels and cardiac arrhythmia, *Nature*, 2006, **440**, 463–469.
- 80 A. E. Prota, F. Danel, F. Bachmann, K. Bargsten, R. M. Buey, J. Pohlmann, S. Reinelt, H. Lane and M. O. Steinmetz, The novel microtubule-destabilizing drug BAL27862 binds to the colchicine site of tubulin with distinct effects on microtubule organization, *J. Mol. Biol.*, 2014, **426**, 1848–1860.
- 81 E. Capdevila, J. Rayo, F. Carrion, I. Jove, J. Borrell and J. Teixido, *Domino and multicomponent (MCR) reactions*, Afinidad, Barcelona, 2003, vol. 60, pp. 317–337.
- 82 L. C. Huan, H. Pham-The, H. Le-Thi-Thu, T. P. Thao, D. N. Que, N.-T. Trang, P. T. Phuong Dung, M. Pyo, S.-B. Han, N. T. Thuan and N.-H. Nam, Exploration of some thiazolidine-2,4-dione and 2-oxoindoline derivatives incorporating 3,4,5-trimethoxybenzyl moiety as novel anticancer agents, *Lett. Drug Des. Discovery*, 2018, **15**, 375–387.
- 83 Q. P. Peterson, D. C. Hsu, D. R. Goode, C. J. Novotny, R. K. Totten and P. J. Hergenrother, Procaspase-3 activation as an anti-cancer strategy: structure-activity relationship of PAC-1, and its cellular co-localization with procaspase-3, *J. Med. Chem.*, 2009, **52**, 5721–5731.
- 84 D.-J. Fu, Y.-F. Zhang, A.-Q. Chang and J. Li,  $\beta$ -Lactams as promising anticancer agents: molecular hybrids, structure activity relationships and potential targets, *Eur. J. Med. Chem.*, 2020, **201**, 112510.
- 85 C. A. Lipinski, F. Lombardo, B. W. Dominy and P. J. Feeney, Experimental and computational approaches to estimate solubility and permeability in drug discovery and development settings, *Adv. Drug Deliv. Rev.*, 2001, **46**, 3–26.

